Gao *et al. Fire Ecology* (2026) 22:57
https://doi.org/10.1186/s42408-026-00474-8

Fire Ecology

RESEARCH

Open Access

Number of dry days drives the expansion of simulated future wildfire in the Florida flatwoods pyrome

Peng Gao[1*], Alex W. Dye[2,3], Karin L. Riley[4] and John B. Kim[5]

Abstract

Background Wildfire activity in the Southeastern United States is shaped by unique ecological and climatic conditions that differ markedly from those in other regions of the country. Despite increasing recognition of fire's ecological importance and rising risks under climate change, regional-scale projections of wildfire behavior in the Southeast remain limited. In this study, we applied the Large Fire Simulator (FSim), a stochastic, spatially explicit fire behavior model, to simulate ignition, spread, suppression, and containment of wildfires within a Florida flatwoods pyrome under both historical and mid-century future climate scenarios. Simulations were driven by fire weather data from 9 downscaled Global Climate Models (GCMs). We evaluated burn probability, fire size, and the number of large fires, and identified key meteorological factors influencing fire dynamics.

Results Simulation results showed substantial variation in projected burn probability across GCMs, with the majority indicating an overall increase. Stepwise regression analysis identified the number of extreme burn days (days when Energy Release Component (ERC) for fuel model G is above the 97th percentile of historical ERC) and the average length of burn blocks (consecutive days when ERC is above the 80th percentile of historical ERC) as the strongest predictors of both region-level burn probability and total area burned. Additionally, the number of burn days and extreme burn days (days when ERC is above the 80th percentile and 97th percentile of historical ERC, respectively) were significantly associated with the number of large fires. Relative humidity and precipitation, rather than temperature alone, emerged as the primary climatic factors that account for fire-conducive conditions. To simplify the interpretation of fire danger, we introduced a "dry day" metric based on thresholds of relative humidity and precipitation, which demonstrated strong predictive power for burn probability in this humid, fuel-rich region.

Conclusions This study found that the number of dry days is the critical factor that accounts for wildfire activity in this region. Our results highlight the importance of incorporating uncertainties in future dry-day projections when developing long-term strategies for wildfire management and adaptation under changing climate conditions.

Keywords FSim, Climate change, Flatwoods, Wildfire modeling, Burn probability, Southeast US, Florida, Global Climate Models

Resumen

Antecedentes La actividad de los incendios de vegetación en el sudeste de los EEUU está modelada por condiciones ecológicas y climáticas únicas, que difieren marcadamente de aquellas que ocurren en otras regiones del país.

*Correspondence:
Peng Gao
gaop@uncw.edu
Full list of author information is available at the end of the article

A pesar del incremento en el reconocimiento sobre la importancia ecológica y el aumento de los riesgos debidos al cambio climático, las proyecciones a escala regional sobre el comportamiento del fuego en el sudeste de EEUU continúan siendo limitadas. En este estudio, aplicamos el simulador de grandes incendios (*Large Fire Simulator*, o FSim), que es un modelo de comportamiento estocástico, espacialmente explícito, para simular la ignición, la propagación, la supresión, y el confinamiento del fuego dentro del área proclive al fuego en los bosques planos de Florida (*Florida Flatwoods*), tanto bajo escenarios de condiciones climáticas históricas como del cambio climático pronosticado a futuro (mediados de este siglo). Las simulaciones fueron corridas mediante el uso de datos meteorológicos tomados de 9 Modelos Climáticos Globales (GCMs) reducidos en escala (d*ownscaled*). Evaluamos la probabilidad de quema, el tamaño de los incendios, y el número de grandes incendios, e identificamos factores meteorológicos clave, que tienen influencia en la dinámica de incendios.

Resultados Los resultados de las simulaciones mostraron una gran variación en la probabilidad proyectada de quema por medio de los GCMs, con la mayoría de ellos indicando un incremento general en las quemas. El análisis de regresión paso a paso identificó el número de días con fuegos o quemas extremas (que son los días en los cuales el Componente de liberación de Energía (ERC), para el modelo de combustible G estuvo por encima del percentil 97 del ERC histórico), y la longitud promedio de los bloques quemados (días consecutivos en los cuales el ERC estuvo por encima del percentil 80 del ERC histórico), como el predictor más fuerte, tanto de la probabilidad de quema a nivel regional como del área total quemada. Adicionalmente, el número de días con fuegos y los días de fuegos extremos (los días en los cuales el ERC está por encima del percentil 80 y del percentil 97 en relación al ERC histórico, respectivamente), estuvieron asociados significativamente con el número de grandes incendios. La humedad relativa y la precipitación, más que la temperatura sola, emergieron como los factores climáticos primarios que favorecieron el desarrollo de los fuegos. Para simplificar la interpretación del peligro de incendio, introdujimos una métrica basada en el "día seco", basada en los límites de humedad relativa y precipitación, las que demostraron un poder predictivo muy fuerte para detectar la probabilidad de incendios en esta región húmeda y rica en combustibles vegetales.

Conclusiones Este estudio encontró que el número de "días secos" es el factor crítico a tener en cuenta para el desarrollo de incendios en esta región. Nuestros resultados subrayan la importancia de incorporar incertidumbres en proyecciones de futuros "días secos" cuando se desarrollan estrategias a largo plazo para el manejo de incendios de vegetación y adaptaciones bajo condiciones climáticas cambiantes.

Background

Wildfires have profound effects on the Southeast U.S., a humid subtropical region characterized by its extensive human-altered landscapes, biological diversity, complex land use patterns, and diverse ownership patterns. As in other regions, wildfires impose direct and sometimes catastrophic impacts on ecosystems (Stevens-Rumann and Morgan 2016) and the environment (Knorr et al. 2017; Brey et al. 2018), threaten human safety and health (Bowman and Johnston 2005; Paveglio et al. 2008; Shankar et al. 2018; Zhang et al. 2023), and cause tremendous economic loss (Duffield et al. 2013; Bayham et al. 2022). However, wildfire also plays an essential role in maintaining native biodiversity and ecosystem functions and processes in this region (Barnett 1999; Mitchell et al. 2014). Historically, the Southeast supported some of the most frequent fire return intervals in North America, shaped by both lightning ignitions and extensive Indigenous cultural burning. Fire-history reconstructions indicate that much of the region burned every 1 to 3 years prior to Euro-American settlement, reflecting a fire regime sustained by warm temperatures, abundant fuels, and persistent human ignitions (Guyette et al. 2012). This deep history of frequent fire underscores its foundational role in structuring the ecosystems of the Southeast.

While the analyses of historical fires suggest the increasing trend of large fires in the Southeast (Donovan et al. 2023), the risk of wildfires in the Southeast is often perceived to be lower than in the Western US, possibly due to the larger and more destructive wildfires and associated economic losses that occur in the West. However, the wildfire risk in the Southeast is significantly higher than the common perception. According to the annual report from the National Interagency Coordination Center, 31% of large fires (>100 acres in timber or >300 acres in grass or brush) in 2024 occurred in the Southeast, more than in any other comparable region (National Interagency Coordination Center 2024). When wildfire risk is understood as a function of hazard, exposure, and vulnerability rather than hazard alone, the Southeast emerges as a region of particular concern. In Florida, for example, Wildland–Urban Interface (WUI) area expanded from approximately 17,732 to 24,722 km^2 between 1990 and 2020, an increase of nearly 40% as development pushed further into fire-prone landscapes (Radeloff et al. 2018; Wildland–Urban Interface (WUI) change by SILVIS Lab (n.d.)). At the same time, many of the most fire-prone areas in the Southeast overlap with some of the poorest and most socially vulnerable rural communities, amplifying potential impacts when wildfires occur (Gaither et al. 2011).

Climate change has further complicated the effects of wildfire in the ecosystems of the Southeast and imposed significant challenges of fire management due to the high biodiversity and accelerated human activities in this region, highlighting the urgent need for strategic planning and proactive measures to mitigate associated risks (Kupfer et al. 2022; Nepal et al. 2023). National- and regional-scale studies on climate change effects on wildfire risk suggest projected longer potential fire seasons (Liu et al. 2013; Brown et al. 2021), greater potential for very large fires (Barbero et al. 2015), increasing burn probability (Gao et al. 2021), and larger burned area (Prestemon et al. 2016) in the Southeast. Moreover, a warming climate is projected to reduce opportunities for prescribed burning, an essential tool that has been used more extensively in the Southeast than in any other region of the USA to reduce fuels and maintain fire-adapted ecosystems (Kupfer et al. 2020). When prescribed burning becomes insufficient, fuels can accumulate rapidly. Combined with increasing aridity, these elevated fuel loads can raise the probability of larger and more intense wildfires. Although many southeastern ecosystems are highly fire-adapted, the growing concern is the heightened risk these wildfires pose to human health and properties and ecosystem services, including carbon stock and water quality (Gaither et al. 2011; Shankar et al. 2018; Hoffman et al. 2023; Pomara et al. 2025).

Statistical analyses and modeling based on the relationships between drought or fire indices and fire activities have been widely used to assess changes in fire potential under a warming climate. For example, Liu et al. (2013) examined future wildfire potential trends across the continental US and found that fire potential measured by the Keetch-Byram Drought Index (KBDI) is projected to increase throughout all four seasons in the Southeast due to rising temperatures. Prestemon et al. (2016) developed a statistical model to project area burned from 2011 to 2060 in the Southeast, incorporating fire-relevant meteorological variables summarized by month, forest land use, and demographic factors. Their model projected increases in both the annual area burned and the total number of wildfires. These statistical approaches are effective at identifying broad trends in fire potential and activity at aggregated temporal (e.g., monthly (Prestemon et al. 2016) or seasonal (Liu et al. 2013)) and spatial scales (e.g., regional, state, or ecoregional level (Prestemon et al. 2016)). However, such aggregations could mask finer-scale variability or worse misconstrue trends due to the importance of daily weather conditions in driving the ignition and spread of large fires. The choice of temporal and spatial aggregation methods requires careful consideration, and there is ongoing debate about which factors most accurately reflect fire danger under these methods (e.g., Fill et al. 2019; Terando et al. 2021). In another example, Bedel et al. (2013) found that while temperature increases are generally consistent across the study area, changes in precipitation, moisture, and atmospheric circulation patterns differ spatially and seasonally, resulting in increased fire potential broadly but with localized exceptions mostly tied to moisture availability. This variability complicates a uniform assessment of future fire risk over the entire Southeastern U.S. These studies underscore the importance of regional and even smaller-scale studies in capturing pyrogeography at finer spatial and temporal scales that reshape regional fire regimes and in identifying the specific factors that drive fire risk in a specific region.

In contrast to statistical models, fire behavior models simulate how wildfire responds to daily weather conditions and spreads across complex topographies and heterogeneous fuel landscapes. These models offer an efficient means of capturing the spatial and temporal variability of fire activity and identifying its underlying drivers (Parisien et al. 2019; Sun et al. 2023). Robbins et al. (2024), for example, used the landscape change model LANDIS-II to explore how climate represented by the daily Canadian Fire Weather Index interacts with fuels and ignition patterns to influence wildfire dynamics and suppression efforts in the Southern Appalachians. Their results revealed substantial spatial variability of fire return intervals driven by fire exclusion and suppression, with some areas experiencing multiple fires per decade while others remained fire-free.

Among the various fire behavior models available, the Large Fire Simulator (FSim) has been widely applied to estimate wildfire risk at national and regional scales under both contemporary and future climate conditions (Riley et al. 2016; Dillon et al. 2023; Dye et al. 2023, 2024; Riley et al. 2025). It has also been used to optimize fire risk management strategies (Scott et al. 2016; Ager et al. 2019, 2020; Thompson et al. 2017) and to compare alternative fire management strategies (Riley et al. 2018), community wildfire protection plans (Hamilton et al. 2024), and to assess wildfire evacuation vulnerability (Dye et al. 2021). FSim's strength lies in its ability to simulate wildfire ignition, spread, suppression, and containment at fine spatial resolutions (typically 90–270 m grid cells) by incorporating topography, fuelscape, and a range of hypothetical fire weather conditions.

Recognizing the spatial variability of fire regimes and the distinct drivers of fire danger in the Southeast, our study focuses on the Florida flatwoods pyrome to examine the impacts of projected climate change on wildfire activity. This pyrome spans a large portion of Florida, a region that experienced a roughly 40% increase in WUI area between 1990 and 2020 (Radeloff et al. 2018; Wildland–Urban Interface (WUI) change by SILVIS Lab (n.d.)). It is also projected to face reduced opportunities for prescribed burning, which could further elevate wildfire risk (Kupfer et al. 2020). We used FSim to simulate wildfire spread across the landscape in this pyrome, driven by daily fire weather derived from multiple downscaled Global Climate Models (GCMs) representing both historical and projected future climates. Our analysis explored the level of agreement among simulations from different GCMs and the meteorological variables most associated with wildfire risk. By addressing these questions, we aim to depict plausible future fire regimes for this region by mid-century under a high warming scenario, providing valuable insights for natural resource planning.

Methods

Study area

The Florida flatwoods pyrome is a ~120,000 km^2 flat plain area covering northern Florida and a small southern portion of Georgia (Fig. 1a). A pyrome is an area that is relatively homogeneous in terms of fire frequency, intensity, size, burned area, and fire season length (Archibald et al. 2013; Short et al. 2020). The vegetation is dominated by longleaf pine savanna (Short et al. 2020). This region contains several protected areas, including multiple National Forests and National Wildlife Refuges. It is also an important center of biodiversity because of its remnant longleaf pine ecosystems, whose persistence is tightly linked to the frequent occurrence of fire (Platt 1999; Rother et al. 2020). At the same time, rapid population growth and urbanization around major cities in the area have driven substantial expansion of the WUI (Radeloff et al. 2018 and Wildland–Urban Interface (WUI) change 1990–2020). The Florida flatwoods pyrome has a mild mid-latitude humid subtropical climate characterized by hot and humid summers and warm to mild winters. The primary fire season is late spring, a window when warm temperatures dry out the fuel before the onset of intense summer humidity.

FSim large fire model

The Large Fire Simulator (FSim) is a spatially explicit fire behavior model that simulates the ignition, spread, containment, and suppression of wildfires on a gridded landscape (Finney et al. 2011) (Fig. S1). FSim is described in detail in prior publications (e.g., Finney et al. 2011; Riley et al. 2016; Dye et al. 2023; Dye et al. 2024). Here, we briefly review its salient features. In FSim, fire activity is driven by the Energy Release Component (ERC) associated with fuel model G, a fuel aridity index defined in the National Fire Danger Rating System (Cohen and Deeming 1985). ERC values are determined by factors including daily temperature, precipitation and its duration, humidity, solar radiation, and the State of Weather (SOW). SOW is a coded National Fire Danger Rating System (NFDRS) variable that represents daily sky and precipitation conditions (from clear skies to thunderstorms). These codes influence fuel moisture calculations and therefore affect ERC. ERC is widely used in wildfire modeling (e.g., Peterson et al. 2021; Wang et al. 2021; Marjani et al. 2023). Generally, as the ERC increases, the probability of ignition also rises (Riley et al. 2013; Riley and Loehman 2016).

FSim simulates ignitions using a two-step process. First, "burn days" are defined as days when ERC is equal to or exceeds the 80th percentile of the historical ERC distribution for that region. This threshold identifies the fire season and reflects the strong relationship between large-fire ignitions and ERC observed across much of the Western US (Riley et al. 2013), a relationship also used in national FSim runs (Dillon et al. 2023). Second, on these burn days, FSim computes the daily ignition probability using a logistic regression model that relates historical large-fire ignitions within the study area to daily ERC values (Andrews et al. 2003; Finney et al. 2011). We applied this same logistic regression framework to evaluate the ERC–ignition relationship for this pyrome.

When ignition is simulated, its location is determined by the Ignition Density Grid (IDG), which is created using historical large fire ignition locations and distributes ignitions proportionately across the landscape. The spread of a fire is modeled using a minimum travel time algorithm that identifies paths with the most rapid fire spread, taking into account factors such as wind, topographic parameters, and fuel characteristics. Another factor affecting wildfire growth is the daily burn period length (hours), which is a function of ERC percentiles. Daily burn hours are 1, 3, and 5 for ERC in the ranges of 80th–89th, 90th–96th, and 97th–100th percentiles, respectively. Fires in FSim stop growing after encountering sustained wet and cool weather conditions exceeding 2 days in non-timber fuels and 5 days in timber fuels. FSim uses daily wind vectors (speed and direction) as a core fire-weather input that influences ignition probability, fire spread, and containment outcomes. Monthly joint distributions of wind speed (binned in 5 mph intervals) and wind direction (binned in 45° intervals) are computed from historical weather records. For each simulation day, FSim randomly samples a single wind vector from the corresponding monthly joint distribution. This

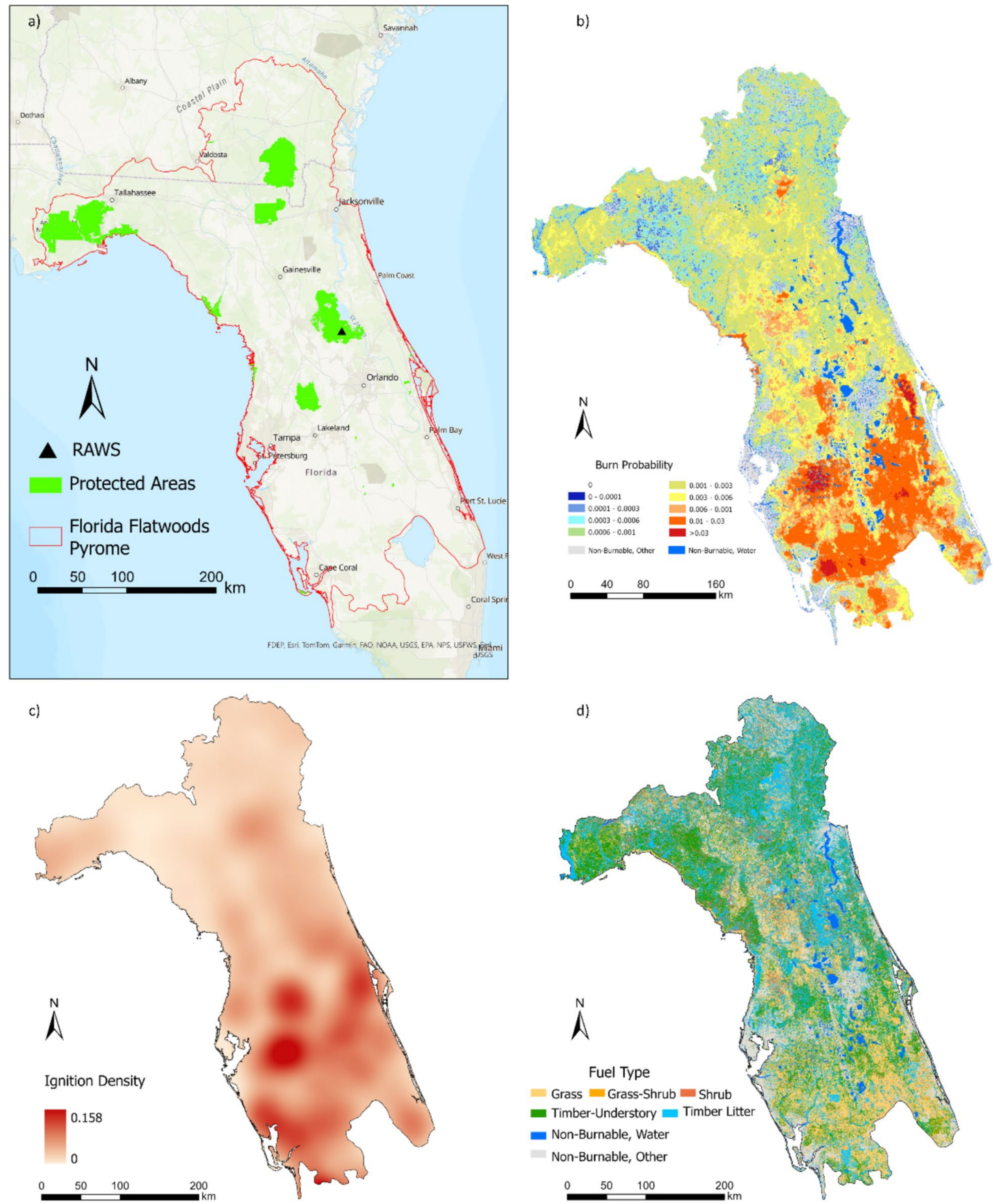

Fig. 1 Simulation domain for the Large Fire Model (FSim) is the Florida flatwoods pyrome covering northern Florida and a small southern portion of Georgia (**a**). Weather data is obtained from the Central Florida Remote Automatic Weather Station (RAWS). Simulation outputs include annual burn probability for the baseline period (1979–2005) (**b**). Ignition Density Grid (IDG) derived from observed ignitions is a key input to the model (**c**). Fuel types are also input, taken from the LANDFIRE program (LANDFIRE 2018) (**d**)

approach does not represent diurnal variability. Instead, the sampled daily wind speed and direction are assumed to remain constant throughout the 24-h simulation period. Additionally, a suppression module can be activated to model the daily containment probability based on vegetation type, time elapsed since ignition, and fire behavior (Finney et al. 2009). Users can also vary a perimeter trimming algorithm to simulate the construction of firelines by fire suppression personnel, which produces realistic fire shapes (Finney et al. 2025).

FSim relies on both dynamic weather data and static spatial data to carry out its simulations. The daily weather data used in this study were either collected at a Remote Automated Weather Station (RAWS) or from downscaled GCMs, depending on the simulation periods discussed in the next sections. The spatial data used in FSim can be categorized into two groups. The first category consists of topographic factors, including elevation, slope, and aspect. The second category encompasses fuel characteristics, such as fire behavior fuel models (Scott and Burgan 2005), canopy bulk density, canopy base height, canopy cover, and canopy height. These spatial data were obtained from the 2016 Remap products from the LANDFIRE program (LANDFIRE 2018) and were resampled to a resolution of 270 m.

At any given spot in the landscape, large fires are infrequent occurrences. The availability and reliability of fire and weather records are limited to a relatively short period of a few decades commencing in 1992 (Short 2014). These records, due to their brief duration, do not provide a comprehensive representation of the diverse combinations of fire weather and ignition patterns. To overcome this limitation, FSim employs a strategy of generating plausible ERC streams for a large number of hypothetical calendar years. Therefore, an FSim run typically simulates wildfire in 10,000 hypothetical calendar years. These ERC streams are derived from statistical properties observed in simulation years (e.g., 1992–2018), including the daily average, standard deviation, and temporal autocorrelation. By simulating fires across these extensive timeframes, FSim encompasses a wide range of possibilities for fire weather conditions.

To assess the likelihood of burning at a specific location, FSim calculates the annual burn probability by determining the number of times that particular pixel experiences fire in the simulations and dividing it by the total number of simulation years. FSim specifically focuses on modeling large fires to maintain computational efficiency, as these fires account for the vast majority of the burned area. In our study, large fires were defined as those with a size of at least 0.3 km^2 (72 acres), equivalent to approximately 4 pixels in the simulation. This threshold was selected to reflect the region's fire regime, which is characterized by frequent, low-intensity, less extensive fires, and to minimize the influence of stochastic variability associated with very small fires. Unless otherwise noted, all references to fire in the following analysis pertain to large fires.

Modeling protocol

Following Dye et al. (2023), we ran FSim for three time periods to produce four sets of simulations which we call *contemporary calibration*, *baseline*, *historical*, and *future* (Table 1). First, we ran FSim for the *contemporary* time period (1992–2018) with observed weather data, using the simulations to calibrate the model to the observed fires in the Fire Occurrence Database (Short 2014, 2021). Second, to produce simulations directly comparable with GCM outputs, we ran FSim with observed weather data for 1979–2005 to create a *baseline* run. While the *contemporary* and *baseline* runs use observed data, the *historical* and *future* runs use downscaled climate projections from GCMs from the MACA-v2-METDATA dataset (Abatzoglou and Brown 2012) under the Representative Concentration Pathway (RCP) 8.5 climate change scenario based on the Coupled Model Intercomparison Project, Phase 5 (CMIP5). We selected future climate projections from 9 GCMs to explore variability across GCMs. Downscaled climate data from GCMs began in 1950, and despite having been bias-corrected

Table 1 Periods and roles of simulation scenarios in the modeling framework (GCMs: Global Climate Models, RAWS: Remote Automatic Weather Station, RCP: Representative Concentration Pathway)

	Climate data	Purpose
Contemporary calibration (1992–2018)	RAWS	Calibrate model settings to reflect observed contemporary fire statistics
Baseline (1979–2005)	RAWS	Simulations covering the historical GCM period for comparison with GCM-based simulations
Historical (1979–2005)	9 GCMs (downscaled MACAv2-METADATA)	GCM-based simulations for the historical period
Future (2040–2069)	9 GCMs (downscaled MACAv2-METADATA)	GCM-based simulations for mid-twenty-first century under RCP8.5 emissions

for major climate features, individual GCMs still exhibit some bias in ERC. To account for those biases, we ran FSim for both *historical* and *future* time periods to enable comparison within each GCM (Table 1). The observed daily weather data were obtained from the Central Florida RAWS located at 29.10° N, −81.62° W (Fig. 1a), and the GCM-based weather time series were extracted at the same location. The same monthly joint distributions of wind speed and wind direction were used in all simulation periods (Table 1). These weather inputs were then applied uniformly across the entire Florida flatwoods pyrome, consistent with the standard FSim configuration in regions (Riley et al., 2016; Dye et al. 2023, 2024).

Contemporary model calibration (1992–2018)

The FSim model was calibrated using observed fire data from the flatwoods pyrome from 1992 to 2018 from the Fire Occurrence Database (FOD) (Short 2021). ERC, which drives fire activities in FSim, was calculated by Fire Family Plus (Bradshaw and McCormick 2009) using the daily weather data from 1992 to 2018 collected at Central Florida RAWS (Fig. 1a). In instances where there were missing values, the gridMet data (Abatzoglou 2013) was employed to fill in the gaps. gridMet is a high-resolution (4-km) gridded dataset widely utilized in ecological modeling for surface meteorological variables (e.g., Balch et al. 2017; Kreider et al. 2024; Zakari et al. 2025), as well as in national FSim runs (Riley et al. 2025; Dillon et al. 2023). The calibration process primarily involved adjusting two parameters: the rate of spread multipliers, which regulate the fire spread across different fuel types, and "acrefract," a divisor number that modifies the probability of a large fire day. The goal of a successful calibration is to ensure that both the mean simulated fire size and the mean number of simulated large fires per year fell within the 70% confidence intervals of the observed means, following standard FSim best practices for model calibration (Scott et al. 2018).

Baseline and historical FSim runs (1979–2005)

To establish a baseline, we conducted an FSim run using observed weather data from 1979 to 2005, collected at the Central RAWS—the same station used for model calibration, augmented with gridMET data where missing values occurred.

For FSim runs in the *historical* climate period, we employed downscaled GCM-based climate data covering the period of 1979–2005, obtained from the MACA-v2-METDATA downscaled climate dataset (Abatzoglou and Brown 2012). MACA-v2-METDATA relies on gridMET as the reference dataset for its downscaling algorithm. "GCM drizzle" is a well-documented problem in GCMs (Sun et al. 2006; Ahlgrimm and Forbes 2014). In the MACAv2-METDATA dataset, it manifests as an unrealistically high frequency of days with extremely light rain that leads to an artificial suppression of ERC values. To rectify this, we excluded the lowest precipitation days from MACAv2-METDATA for the historical period to align the number of drizzle days within the 95% confidence interval of those at the RAWS for the baseline period, considering the baseline period as the reference for accurate values for each month (Supplement). The adjustments induced little change in monthly precipitation totals (Table S1), while reducing the number of days with precipitation. Precipitation duration and SOW, the two variables required in the calculation of ERC, are not available in the MACA-v2-METDATA. The former was estimated by the method based on the empirical relationship between precipitation depth and duration described in Abatzoglou and Kolden (2013). The latter was calculated based on precipitation duration and percent of cloud cover, where cloud cover was inferred from the ratio between solar radiation and potential maximum radiation (Table S2). Subsequently, we compared the simulation results from the *historical* period with those from the *baseline* period to interpret any potential biases present in GCMs. The 1979–2005 timeframe was chosen as it overlaps with the standard historical period covered by the GCM-based climate data.

Future FSim runs (2040–2069)

For this study, we focused on the mid-century period (2040–2069) characterized by the RCP8.5 high-warming climate change scenario to investigate the impacts of climate change. Although RCP 8.5 represents a very high emissions pathway, Bayesian analyses suggest that it remains highly plausible through approximately 2060 (Huard et al. 2022). We retained the same landscape for all FSim runs so that we can isolate the effects of climate change on fire activities from the interference of concurrent alterations in vegetation and maintain the clarity of the climate signal. To account for "GCM drizzle" in the projected ERC calculations, we applied similar adjustments as in the historical period. However, the target number of drizzle days for the future period was modified based on the ratio of unadjusted drizzle days in the future period to those in the historical period (Supplement). This adjustment procedure had only minimal impacts on total precipitation values (Table S3), while reducing the number of drizzle days. In subsequent analyses, we compared simulation results from the *future* period (2040–2069) with those from the *historical* period (1979–2005) to interpret projected changes within each GCM for the future climate scenario.

We evaluated burn probability at two spatial scales. First, at the pixel level, burn probability was calculated at the 270-m FSim grid resolution as the fraction of simulated years in which each pixel burned. Second, at the region level, burn probability was computed as the spatial mean of pixel-level burn probabilities across the entire study area. We refer to these as pixel-level burn probability and region-level burn probability, respectively.

Impacts of climate change on wildfire activities

To assess the impacts of climate change on wildfire activities in this region, we analyzed historical and future burn probabilities simulated with nine GCMs. Our analyses proceeded in three components.

First, we examined how region-level burn probability relates to two key fire outcomes: total area burned and the number of fires. We also quantified changes in region-level burn probability, average fire size, and the number of fires from the historical period to the future period.

Second, we evaluated how burn-day dynamics—the number of burn days and their temporal structure—shape wildfire activity in this region. Specifically, we examined how these dynamics relate to (1) region-level burn probability, (2) total area burned, and (3) the number of fires. In FSim, fires can only ignite on "burn days"—defined as days when ERC equals or exceeds the 80th percentile of historical values—making the number of burn days a direct determinant of burn probability. Strong correlations between the number of burn days and burn probability have been reported in Southern California (Dye et al. 2023) and the Pacific Northwest (personal communication with Dye et al. 2024). To further quantify the temporal distribution of burn days, we developed the metric "average length of burn blocks," where a burn block is a continuous sequence of one or more consecutive burn days. This metric is calculated as the total number of burn days divided by the number of burn blocks within a given period.

To capture varying degrees of fire-conducive conditions, we classified burn days and burn blocks into three categories based on ERC thresholds: burn days (≥80th percentile), high burn days (≥90th percentile), and extreme burn days (≥97th percentile). We then conducted a stepwise multivariate linear regression using six variables—the number of burn days and the average length of burn blocks at each of the three ERC levels defined by thresholds (i.e., ≥80th percentile, ≥90th percentile, and ≥97th percentile)—to identify which factors significantly explained variations in region-level burn probability.

Third, because ERC integrates multiple weather inputs and is therefore less intuitive than direct meteorological variables, we further investigated the relationship between three primitive meteorological variables (i.e., temperature, relative humidity, and precipitation) and the number of burn days that contributed to region-level burn probability. This analysis was conducted to link fire danger metrics back to primitive meteorological variables that are more tangible and broadly interpretable. Meteorological variables influence burn probability only indirectly through their effects on ERC and the resulting burn-day structure; therefore, evaluating weather–ERC linkages clarifies the first step in the causal chain. Since ERC incorporates the 1000-h equilibrium fuel moisture, which is influenced by a 7-day running mean boundary condition of weather conditions (Cohen and Deeming 1985), we calculated the 7-day running means of temperature, relative humidity, and precipitation. We then compared the distributions of the three smoothed variables on burn days, high burn days, and extreme burn days defined by ERC thresholds versus days that did not meet these thresholds. To identify dry conditions, we extracted the 90th percentile thresholds for the three variables and defined a dry day as any day meeting two of the following three criteria: temperature exceeding its threshold, or relative humidity or precipitation falling below their respective thresholds. We evaluated which combination of these criteria for defining a dry day produced the strongest correlation with region-level burn probability.

Selection of GCMs for historical and future scenarios

Running FSim is computationally expensive. For example, a single FSim simulation of 10,000 iterations (hypothetical years) for this pyrome required approximately 2–3 weeks to complete on a multicore server. The computing environment consisted of a single-socket AMD EPYC 7702P processor with 64 physical cores (SMT disabled), 64 logical processors, and 256 GB of RAM. To make computing manageable for this study, we selected 9 GCMs from the 18 available GCMs downscaled by MACAv2-METDATA (Abatzoglou and Brown 2012). Previous studies suggested a strong correlation between burn probability and the number of burn days (Dye et al. 2023). Therefore, we used the number of burn days as a proxy to choose the 9 GCMs that cover the similar ranges of bias and change of burn probability suggested by all 18 GCMs. We estimated the region-level burn probability from the other 9 GCMs that we did not perform FSim simulation using significant variables identified in this study that account for burn probability. To ensure the 9 selected GCMs captured the similar ranges of bias, change, and variance of burn probability suggested by all 18 GCMs, we compared the mean and the distribution of the burn probability from the 9 selected GCMs and the unselected 9 GCMs in the historical and future periods using a *t*-test (Student 1908), a Kruskal–Wallis test (Kruskal and Wallis 1952), and a Levene's test (Levene

1960), respectively. If the two tests suggest no significant difference, it is reasonable to conclude that the 9 GCMs captured the bias and change of burn probability suggested by all 18 GCMs.

Results

Contemporary model calibration (1992–2018)

The calibrated FSim model produced an average of 166.8 large fires per year, with an average burned area of 4.2 km^2 per year from 1992 to 2018. These values are closely aligned with the observed records from the FOD, which reported an average of 168.9 large fires per year and an average burned area of 4.0 km^2 per year, and fell within the 70% confidence intervals of 157.9 to 196.4 fires per million acres per year and 3.5 to 4.4 km^2 per year, respectively. Although the frequency and size of simulated large fires deviate from the observed record in some months, overall, the seasonality of simulated large fires follows that of the observed records. The primary discrepancies include a notable underestimation of burned area in April, underestimation of the number of large wildfires in January and February, and a slight overestimation during the summer months (Fig. 2).

Baseline simulation (1979–2005)

The baseline run yielded the same fire frequency as that of the calibration run (166.8 large fires per year) but a smaller average burned area of 3.7 km^2 per year, and followed the seasonality of simulated fires in the calibration run, except that the calibration had the larger burned area in March (Fig. 2a). The region-level burn probability is 0.0049 (Table 2). Areas with high burn probability generally align with regions of historically high ignition density and fuel types characterized by high rates of spread. These included grass, which covers 27% of the study area and is concentrated in the southern region and a strip along the western centre, and timber-understory, which comprises 21% of the area and is mainly found in the northern region (Fig. 1 and Fig. S2).

Historical FSim runs and bias in burn probability

The number of GCMs that overestimated versus underestimated region-level burn probability in the historical period was roughly equal. Four GCMs—CanESM2, GFDL-ESM2G, GFDL-ESM2M, and MIROC-ESM-CHEM—produced a positive bias, while the remaining five—bcc-csm1-1, CNRM-CM5, CSIRO-Mk3-6-0, IPSL-CM5A-LR, and MRI-CGCM3—exhibited a negative bias. Among these, GFDL-ESM2M showed the greatest overestimation at 0.0026, whereas bcc-csm1-1 and MRI-CGCM3 had the largest underestimations at −0.001 (Table 2). Notably, areas with high historical burn probability in the southern half of the study area tended to exhibit larger biases regardless of direction. At the pixel level, bias varied spatially, with both overestimations and underestimations occurring within individual GCM runs (Fig. S3).

A pixel-level bias range of 0.002 (off by 2 fires in 1000 hypothetical years) can be considered acceptable and could be attributable to the inherent stochasticity of the FSim model. Among the 9 GCM runs, six of them (bcc-csm1-1, CNRM-CM5, CSIRO-Mk3-6-0, IPSL-CM5A-LR, MIROC-ESM-CHEM, and MRI-CGCM3) showed at least 78% of the region area having biases within this acceptable range. Even GFDL-ESM2M, which had the highest overestimation, had 63% of its landscape area within the 0.002 range. These results indicate that the GCMs reproduced the general fire weather conditions for the inputs of the FSim model.

Future FSim runs and change in burn probability

Among the nine future FSim runs, six GCMs—bcc-csm1-1, CNRM-CM5, CSIRO-Mk3-6-0, GFDL-ESM2G, IPSL-CM5A-LR, and MIROC-ESM-CHEM—projected an increase in region-level burn probability, while the remaining three—CanESM2, GFDL-ESM2M, and MRI-CGCM3—projected a decrease. The mean increase across the six GCMs was 0.0014 (40.57%), whereas the mean decrease across the three GCMs was −0.0009 (−19.29%). IPSL-CM5A-LR produced both the largest absolute increase (0.0043) and the largest relative increase (119.44%). In contrast, GFDL-ESM2M exhibited the largest absolute decrease (−0.0016), while MRI-CGCM3 showed the largest relative decrease (−29.03%) (Table 2). Regardless of whether the region-level change was positive or negative, both increases and decreases occurred at the pixel level within each GCM run, reflecting the spatial variability and stochasticity of burn probability. Large absolute increases and decreases were concentrated in areas and fuel types with historically high burn probability; however, these areas generally experienced smaller relative changes—except for IPSL-CM5A-LR, where the substantial absolute increase also resulted in a large relative increase (Figs. S2, S4, and S5).

We found no clear correlation between the bias and the projected change of these GCMs (Fig. S6). To facilitate the interpretation of burn probability suggested by these GCMs, we took the average of the 6 GCMs (i.e., bcc-csm1-1, CNRM-CM5, CSIRO-Mk3-6-0, IPSL-CM5A-LR, MIROC-ESM-CHEM, and MRI-CGCM3) that had at least 78% of the burnable area having pixel-level biases within this acceptable range of ±0.002 and whose region-level bias was in the range of ±0.001. The 6 GCMs cover almost the full range of changes suggested by all the 9 GCMs (Table 2). The mean region-level

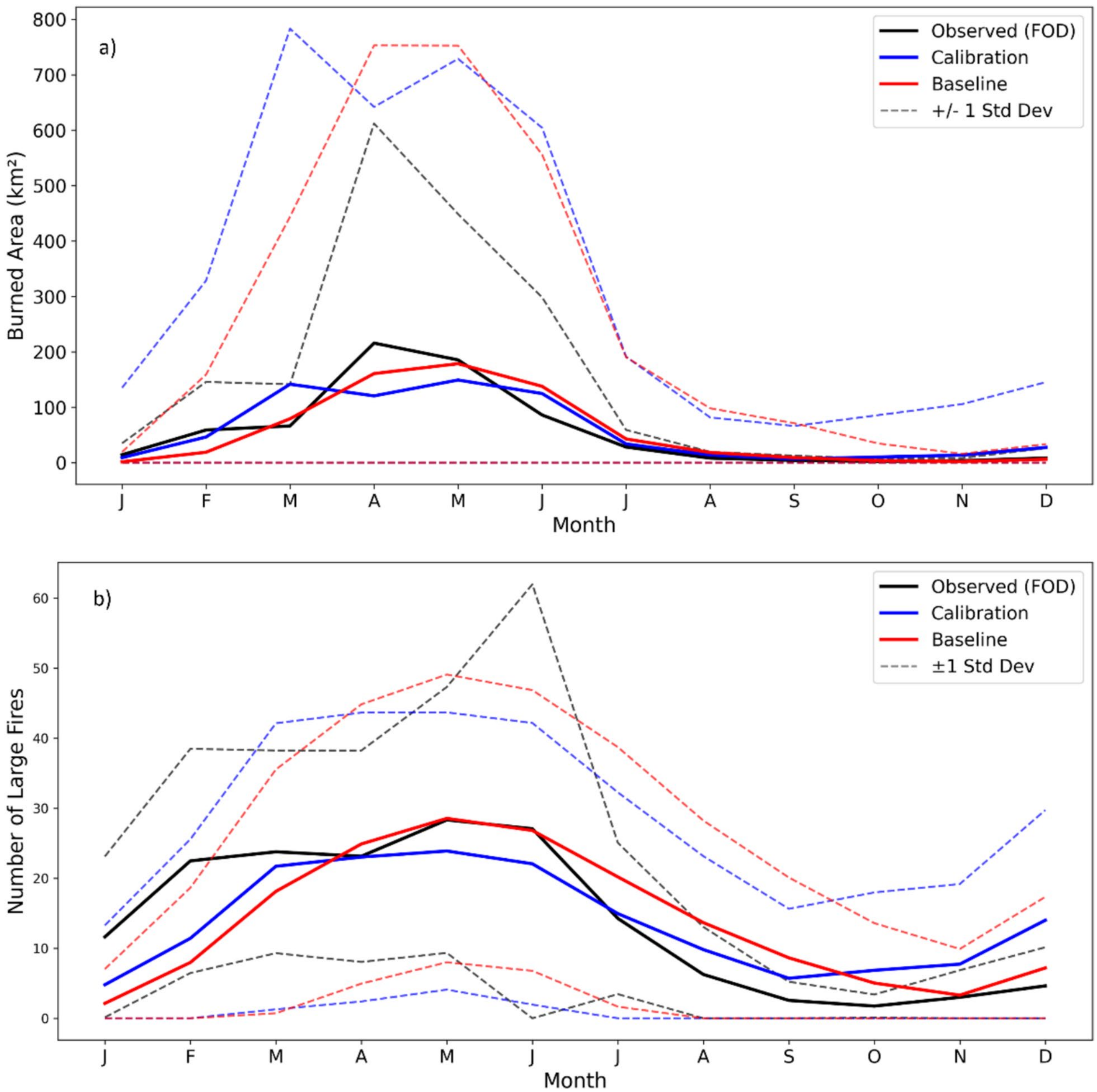

Fig. 2 Simulated burned area vs. observed (**a**) and simulated number of large fires vs. observed (**b**). Observed burned area and number of large fires are calculated from observations in the Fire Occurrence Database (FOD) from 1992 to 2018 (Short 2021). The calibration run represents 1992 to 2018, and the baseline run represents 1979–2005. Solid lines represent monthly means, and dash lines indicate one standard deviation

burn probability of historical runs (0.0035) was close to that of the baseline run (0.0041), which suggested that historical fire weather from GCMs that drivers of area burned and number of large fires were likely not largely different from those observed in the RAWS data. Most burnable areas are projected to increase in burn probability in the future timestep (Fig. S7). The region-level burn probability is projected to have an increase of 0.0013 (35.55%).

Impacts of climate change on wildfire activities

Region-level burn probability, area burned, and the number of fires

As expected, there was a positive correlation among region-level burn probability, area burned, and the

Table 2 Region-level burn probability of baseline run based on the Central Florida Remote Automatic Weather Station (RAWS), and historical and future FSim runs for 9 Global Climate Models (GCMs). Six bolded GCM runs have very low bias compared to the baseline run, ≤ ±0.001

GCMs	Historical (1979–2005)	Bias compared to baseline	Future (2040–2069)	Absolute change	Relative change
bcc-csm1-1	**0.0031**	**−0.0010**	**0.0039**	**0.0008**	**25.81%**
CanESM2	0.0057	0.0016	0.0054	−0.0003	−5.26%
CNRM-CM5	**0.0033**	**−0.0008**	**0.0042**	**0.0009**	**27.27%**
CSIRO-Mk3-6-0	**0.0035**	**−0.0006**	**0.0057**	**0.0022**	**62.98%**
GFDL-ESM2G	0.0058	0.0017	0.0060	0.0002	3.45%
GFDL-ESM2M	0.0067	0.0026	0.0051	−0.0016	−23.58%
IPSL-CM5A-LR	**0.0036**	**−0.0005**	**0.0079**	**0.0043**	**119.44%**
MIROC-ESM-CHEM	**0.0045**	**0.0004**	**0.0047**	**0.0002**	**4.44%**
MRI-CGCM3	**0.0031**	**−0.0010**	**0.0022**	**−0.0009**	**−29.03%**
	Baseline (1979–2005)				
RAWS	0.0041				
6 low-bias GCM mean	0.0035		0.0048	0.0013	35.55%
9 GCM mean	0.0044		0.0050	0.0006	14.76%

number of fires. The correlation between burn probability and area burned was particularly strong ($R^2 = 0.991$, $p < 0.01$), whereas the correlation between area burned and the number of fires was less strong but still significant ($R^2 = 0.5208$, $p < 0.01$). This stronger correlation is likely because the annual burn probability—calculated as the frequency of all fires that occurred at a particular location across simulations divided by the total number of simulation years—is directly related to the area burned. In contrast, the area burned is influenced not only by the number of fires but also by their sizes.

Among the 9 GCMs, three (i.e., CanESM2, GFDL-ESM2M, and MRI-CGCM3) indicated a decrease in area burned and burn probability, all of which corresponded with a reduction in average fire size (Fig. 3). In the case of CanESM2, the effect of the decreasing average fire size was offset by an increase in the number of large fires. For GFDL-ESM2M, the decrease in area burned and burn probability was primarily due to a reduction in average fire size; despite a slight decrease in the number of large fires, from 170.6 to 169.7 (a 0.5% decrease), the area burned by large fires dropped by over 20%, from 1065 to 827 km^2. For MRI-CGCM3, the decrease in area burned and burn probability was due to reductions in both the average fire size and the number of large fires. For the remaining 6 GCMs (i.e., bcc-csm1-1, CNRM-CM5, CSIRO-Mk3-6-0, GFDL-ESM2G, IPSL-CM5A-LR, and MIROC-ESM-CHEM), all of which projected an increase in area burned and burn probability, each showed an increase in the number of large fires. However, in the cases of GFDL-ESM2G and MIROC-ESM-CHEM, this effect was largely offset by a decrease in fire size (Fig. 3).

Impact of burn-day dynamics on region-level burn probability, area burned, and the number of fires

The stepwise multivariable linear regression based on data from 9 GCMs across historical and future periods yielded consistent findings for both region-level burn probability and area burned, because the two are highly correlated. The results indicated that extreme burn days ($p < 0.01$) and the average length of burn blocks ($p < 0.01$) together explained a substantial portion of the variation in burn probability and area burned (adjusted $R^2 = 87.0\%$, $p < 0.01$, Fig. 4). Extreme burn days held relatively higher importance than the average length of burn blocks (62.0% vs. 38.0%). Higher numbers of burn days and longer burn blocks are associated with increased burn probability. For 5 GCMs (CNRM-CM5, CSIRO-Mk3-6-0, GFDL-ESM2M, IPSL-CM5A-LR, and MRI-CGCM3), burn probability changed in the same direction as both extreme burn days and average burn block length. For the remaining 4 GCMs (bcc-csm1-1, CanESM2, GFDL-ESM2G, and MIROC-ESM-CHEM), extreme burn days increased while the average burn block length decreased. In these cases, burn probability generally increased in response to more extreme burn days, except for CanESM2, where the decline in burn block length outweighed the increase in extreme burn days, leading to a net decrease in burn probability (Fig. 5a). The same trends were observed for area burned (Fig. 5b).

Logistic regression indicated a strong and significant relationship between ERC values and the probability of large fire occurrence ($p < 0.01$, pseudo $R^2 = 0.98$). The estimated probability of a large fire was 0.67 at the 80th percentile of ERC values and increased substantially when

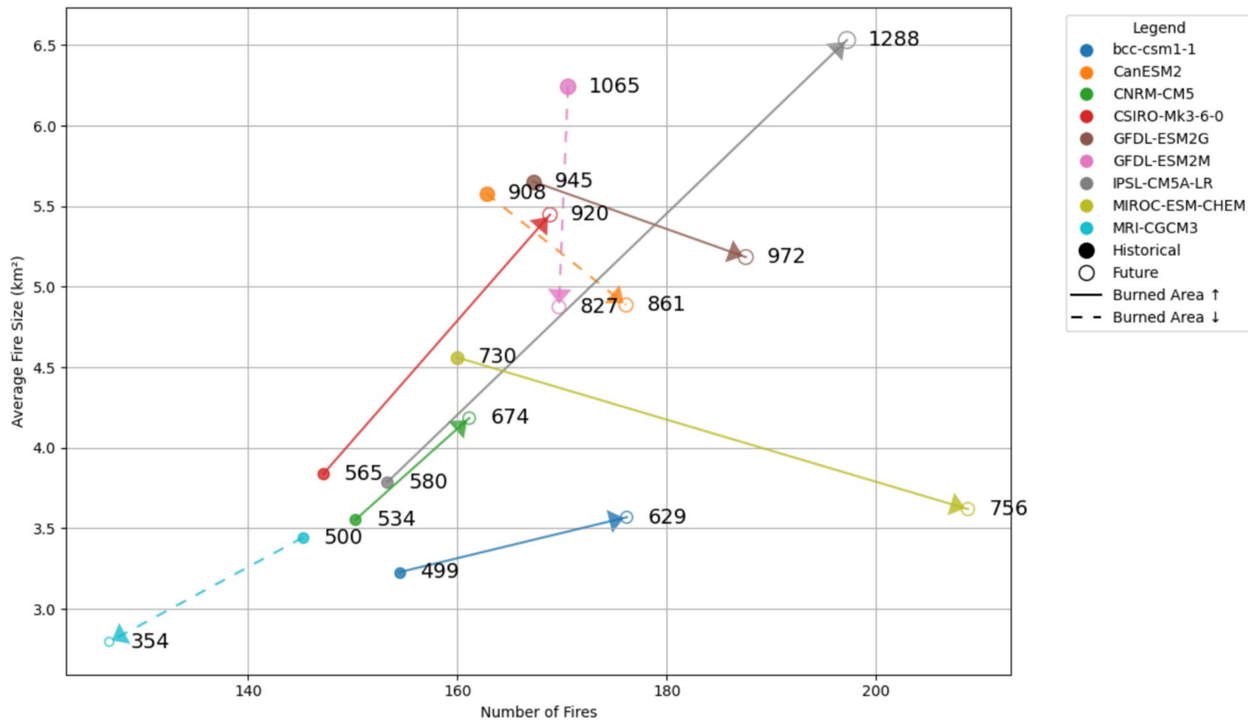

Fig. 3 Change in number of fires (x-axis), average fire size (y-axis), and total burned area (km^2) (proportional to marker size and also denoted by numbers adjacent to markers) from the historical (1979–2005) to future (2040–2069) in FSim simulations driven with 9 Global Climate Models (GCMs). Solid and dashed lines connect markers for each GCM, from historical to future. Dashed lines indicate decreases in burned areas from historical to future, while solid lines indicate increases

ERC exceeded this threshold. The stepwise multivariable linear regression indicated the number of large fires had a strong correlation with the burn days and extreme burn days (the adjusted $R^2 = 0.8756$, p value < 0.01) (Fig. 6). The relative importance of the former and the latter was 55% and 45%. Among 7 of 9 GCMs including bcc-csm1-1, CanESM2, CNRM-CM5, CSIRO-Mk3-6-0, GFDL-ESM2G, IPSL-CM5A-LR, and MIROC-ESM-CHEM, the number of large fires increased as the burn days and the extreme burn days increased, while the number of large fires from MRI-CGCM3 decreased, as the burn days and the extreme burn days decreased. For GFDL-ESM2M, the effect of the increased number of burn days was offset by the decrease in the number of extreme burn days, resulting in a slight decrease in the number of large fires (Fig. 7).

Primitive meteorological variables and region-level burn probability

Because the number of extreme burn days was statistically significant in explaining burn probability, total burned area, and the number of large fires, we examined its relationship with three fundamental meteorological variables (i.e., temperature, relative humidity, and precipitation). We found that 90% of extreme burn days occurred when the 7-day running mean of temperature exceeded 27.8 °C, relative humidity fell below 64.0%, and precipitation was less than 1.4 mm.

The distributions of the seven-day running mean of relative humidity and precipitation based on 9 GCMs in historical and future periods display a clear demarcation between extreme burn days and non-extreme burn days (Fig. S8a and b). In contrast, the distribution of the 7-day running mean of temperature shows a minimal distinction between extreme burn days and non-extreme burn days (Fig. S8c). Although all GCMs project higher temperatures (Fig. S9), changes in burn probability vary (Table 2), suggesting that temperature alone has limited explanatory power for burn probability. Changes in relative humidity are generally more pronounced than those in precipitation. Notably, 6 GCMs, including bcc-csm1-1, CNRM-CM5, CSIRO-Mk3-6-0, GFDL-ESM2G, IPSL-CM5A-LR, and MIROC-ESM-CHEM, show increased frequencies of days with relative humidity below 64.0% from January to April, coinciding with their projected increases in burn probability. This pattern is especially evident for CSIRO-Mk3-6-0 and IPSL-CM5A-LR, which show the largest increases in burn probability. Conversely, GFDL-ESM2M, which projects the greatest decrease in burn probability, exhibits fewer days with

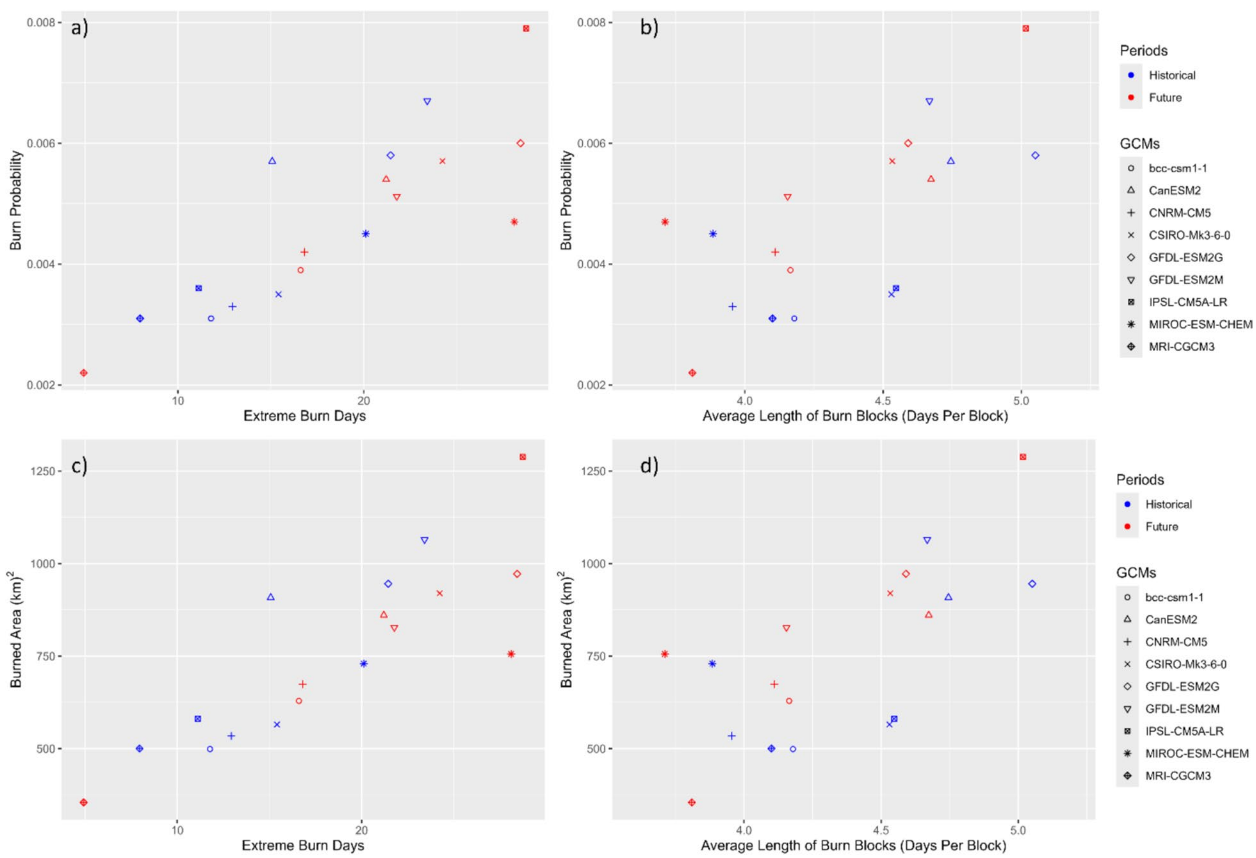

Fig. 4 The relationship of the number of extreme burn days versus region-level burn probability (**a**), length of burn blocks versus region-level burn probability (**b**), number of extreme burn days versus burned area (**c**), and length of burn blocks versus burned area (**d**), as suggested by stepwise linear regression. Extreme burn days are days when the Energy Release Component (ERC) is ≥97th percentile. A burn block is a continuous sequence of one or more consecutive days when ERC exceeds the 80th percentile, which allows for fire to be ignited. Each Global Climate Model (GCM) run is represented by two markers of the same shape, a blue marker for the historical period (1979–2005) and a red marker for the future (2040–2069)

relative humidity below 64.0% during the same period. The remaining two (i.e., CanESM2 and MRI-CGCM3) display less consistent changes in relative humidity and precipitation (Fig. S10)

Among the three criteria combinations used to define dry days, the strongest correlations with extreme burn days were found when both the 7-day running mean of relative humidity and precipitation fell below 64.0% and 1.4 mm, respectively, the same thresholds that were identified earlier as characterizing 90% of extreme burn days ($R^2 = 0.73$, $p < 0.01$, Fig. 8a). This combination outperformed the relative humidity–temperature ($R^2 = 0.28$) and temperature–precipitation ($R^2 = 0.04$) criteria. The number of dry days defined by the relative humidity–precipitation combination was also strongly correlated with burn days ($R^2 = 0.85$, $p < 0.01$, Fig. 8b). These strong relationships are expected, as extreme burn days represent a subset of burn days. Importantly, the number of dry days also exhibited strong predictive power for region-level burn probability ($R^2 = 0.53$, $p < 0.01$; Fig. 9).

Finally, we estimated the region-level burn probabilities for the 9 GCMs not simulated with FSim by using two empirical relationships: (1) burn probability with the number of extreme burn days and the length of burn blocks and (2) burn probability with the number of dry days. Results from both the *t*-test and Kruskal–Wallis test indicated no significant differences in either the means or the distributions between the 9 GCMs simulated with FSim and the 9 GCMs estimated from these relationships (Table 3). This suggests that the selected nine GCMs reasonably captured both bias and the projected changes in burn probability across all 18 GCMs.

Discussion

Implications of GCMs for burn probability projections

Similar to other simulation-based studies that incorporate multiple climate projections (e.g., Barros et al. 2021; Heidari et al. 2021; McEvoy et al. 2021; Dye et al. 2023, 2024), we also observed considerable variability in FSim outcomes depending on the GCMs used to drive FSim

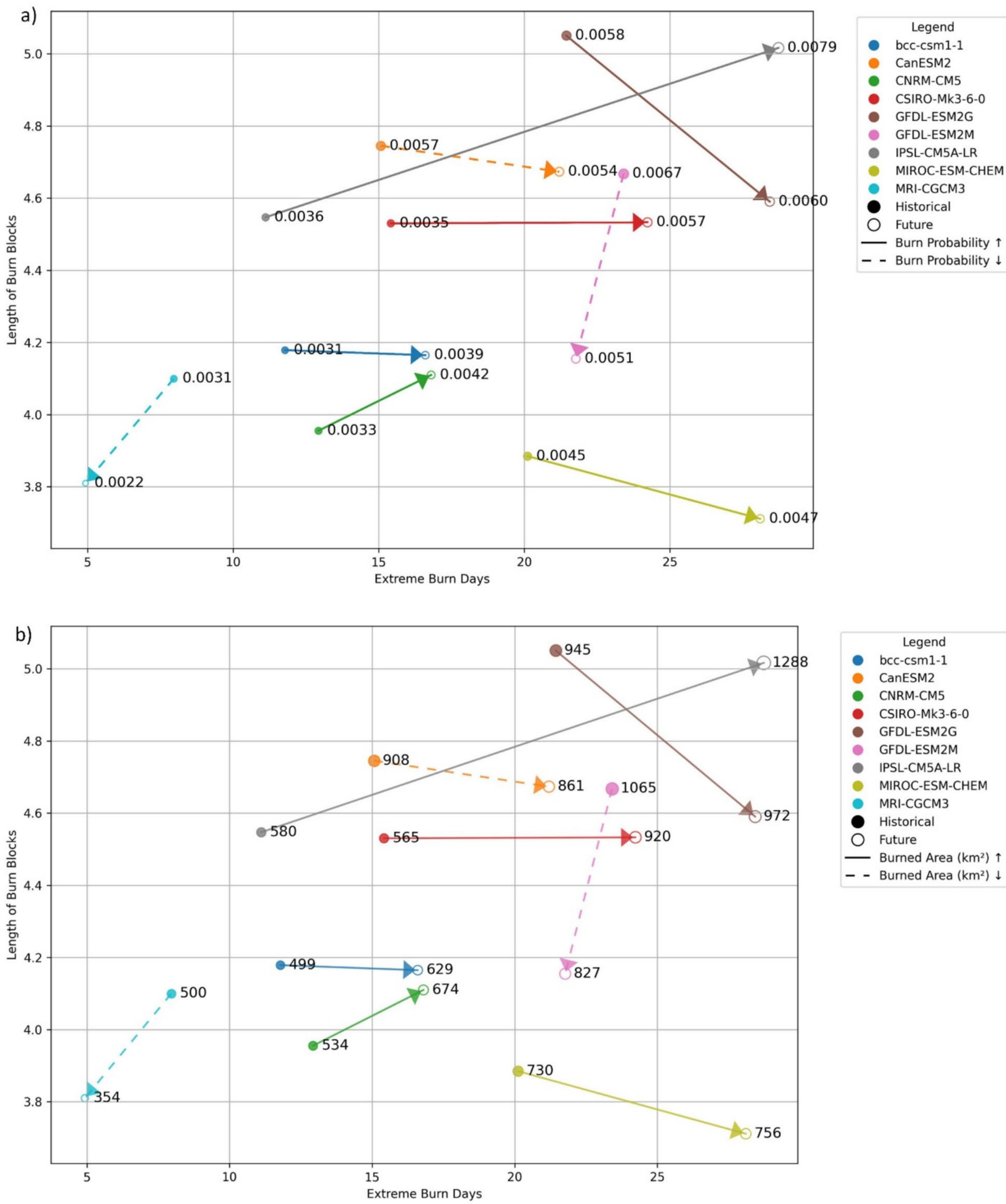

Fig. 5 Shifting relationship between extreme burn days (x-axis), the length of burn blocks (y-axis), and burn probability (**a**) and burned area (**b**) (proportional to marker size and also denoted by numbers adjacent to markers) from the historical (1979–2005) to future (2040–2069) in FSim simulations driven with 9 Global Climate Models (GCMs). Solid and dashed lines connect markers for each GCM, from historical to future. Dashed lines indicate decreases in burn probability (**a**) and burned area (**b**) from historical to future, while solid lines indicate increases

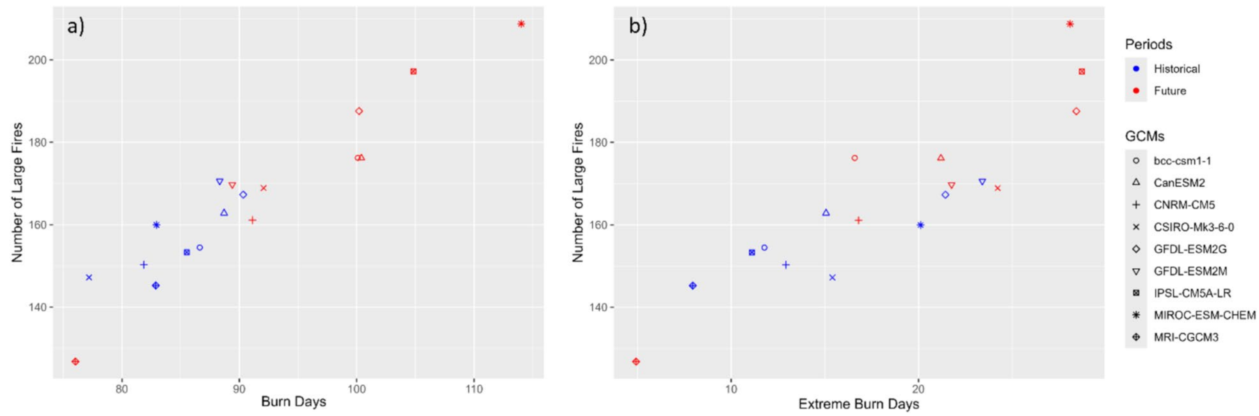

Fig. 6 Stepwise linear regression identifies correlations between the number of burn days (Energy Release Component (ERC) ≥ 80th percentile) (**a**) and extreme burn days (ERC ≥ 97th percentile) (**b**), and the number of simulated large fires. Each Global Climate Model (GCM) run is represented by two markers of the same shape, a blue marker for the historical period (1979–2005) and a red marker for the future (2040–2069)

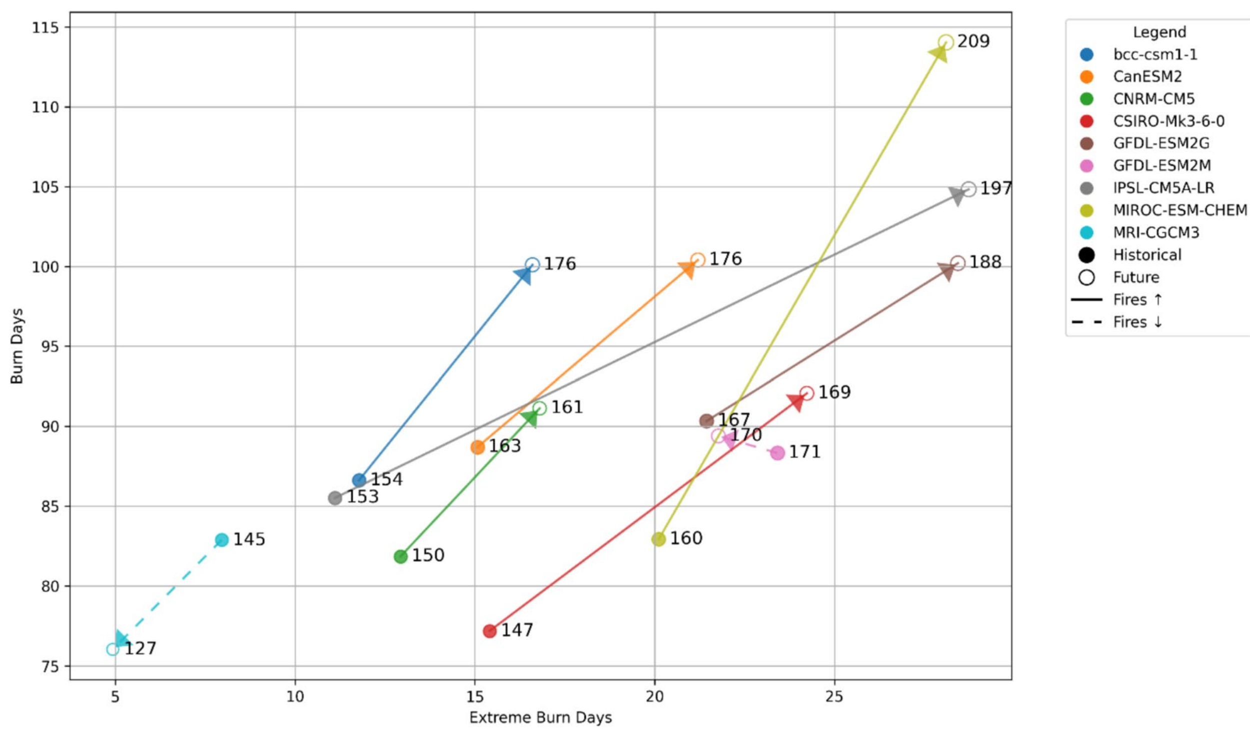

Fig. 7 Shifting relationship between extreme burn days (x-axis), burn days (y-axis), and the number of large fires (proportional to marker size and also denoted by numbers adjacent to markers) from the historical (1979–2005) to future (2040–2069) in FSim simulations driven with 9 Global Climate Models (GCMs). Burn days and extreme burn days are when the Energy Release Component (ERC) exceeds 80th and 97th percentile, respectively. Dashed and solid lines connect markers for each GCM, from historical to future. Dashed lines indicate decreases in the number of large fires from historical to future, while solid lines indicate increases

inputs. Using multiple GCMs is a widely recommended best practice for analyzing future climate impacts (e.g., Mote et al. 2011 recommend 10 or more), although resource constraints may limit the number used in some studies. In our analysis, we included 9 GCMs to capture variability in model bias when reproducing historical burn probabilities and to reflect the uncertainty inherent in future climate projections. Although projected changes in burn probability differ across individual models, the majority of GCMs (6 out of 9) suggest increased burn probability. Moreover, both the multi-model average across all nine GCMs and the average across the

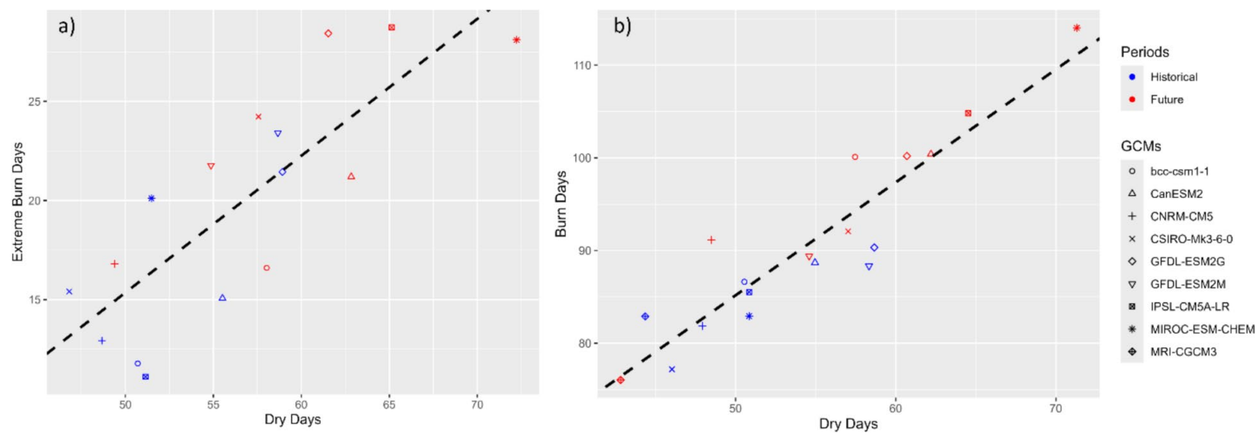

Fig. 8 Linear correlations between the number of dry days and the number of extreme burn days when Energy Release Component (ERC) exceeds 97th percentile (**a**), and the number of burn days when ERC exceeds 80th percentile (**b**). Each Global Climate Model (GCM) run is represented by two markers of the same shape, a blue marker for the historical period (1979–2005) and a red marker for the future (2040–2069)

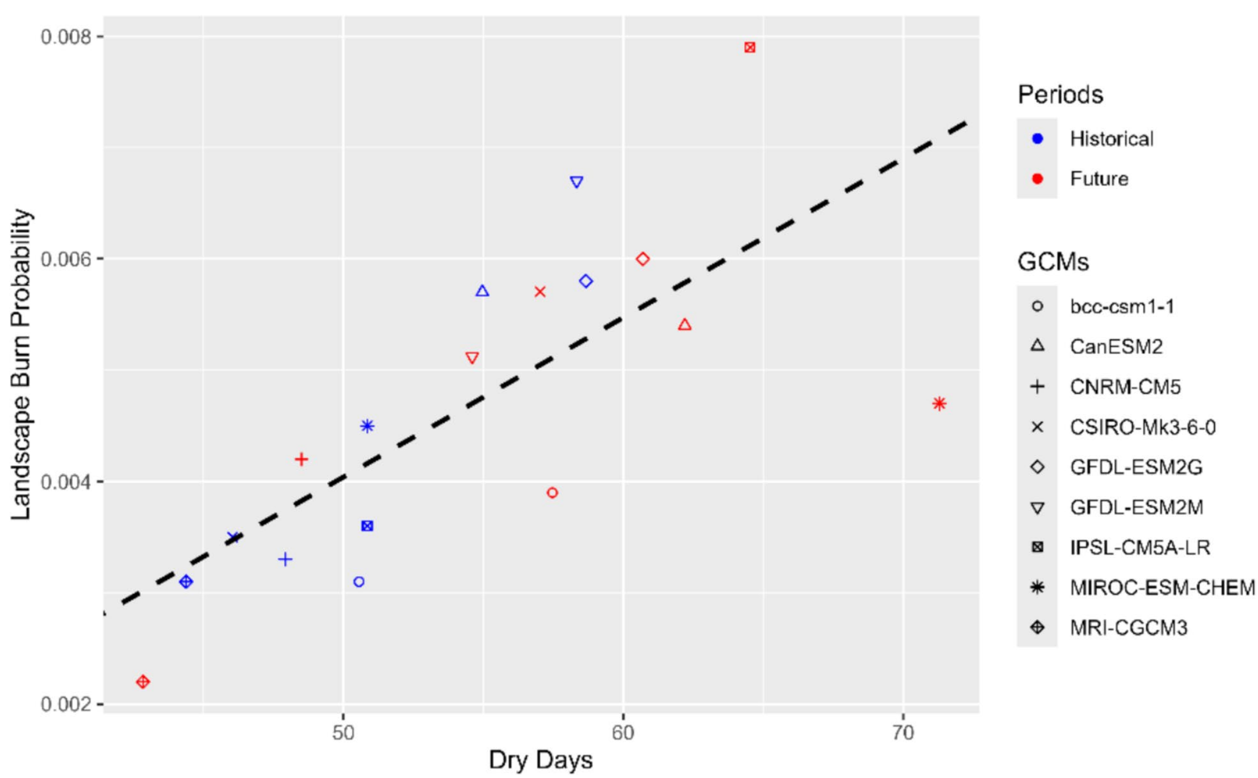

Fig. 9 Linear correlation between the number of dry days and region-level burn probability. Each Global Climate Model (GCM) run is represented by two markers of the same shape, a blue marker for the historical period (1979–2005) and a red marker for the future (2040–2069)

six GCMs with lower historical bias indicate an overall increase in burn probability. The findings align with other regional and national studies forecasting elevated fire risk in this region (e.g., Brown et al. 2021; Liu et al. 2013; Barbero et al. 2015; Prestemon et al. 2016; Gao et al. 2021). While the absolute changes appear small, the relative changes are substantial because burn probability can be directly translated to burned area.

Intriguingly, some GCMs with positive biases in historical simulations—most notably CanESM2 and GFDL-ESM2M—project decreases in both area burned and burn probability in the future. On continental to

Table 3 Comparison of region-level burn probabilities simulated with FSim and estimated from empirical relationships in the historical and future periods. *Estimation1* is based on the relationship with the number of extreme burn days and the length of burn blocks, while *Estimation2* is based on the relationship with the number of dry days

		FSim simulated	Estimation1	Estimation2
Historical	Mean	0.0044	0.0040	0.0040
	Median	0.0036	0.0035	0.0038
	Variation	1.87E−06	2.55E−06	1.15E−06
Future	Mean	0.0050	0.0053	0.0058
	Median	0.0051	0.0062	0.0058
	Variation	2.48E−06	2.82E−06	1.90E−06

global scales, it is reasonable to expect positive present-day biases in GCMs (e.g., warmer temperatures) to persist into future projections. However, our FSim simulations are run for a single pyrome, driven with an ERC stream representative for the pyrome. ERC values used in our simulations are highly sensitive to regional-scale moisture transport and precipitation patterns simulated by GCMs. As a result, a GCM that exhibits a positive ERC bias during the historical period can still project lower ERC in the future if it simulates increases in relative humidity or precipitation that suppress fuel drying. This appears to be the case for these two GCMs, which project a warmer but more humid and wetter future climate in this pyrome despite warmer temperatures, leading to reduced fire potential. Under alternative modeling protocols that apply projected climate anomalies to observed weather (e.g., Riley and Loehman 2016), the influence of such baseline biases would likely be muted, and projected changes in fire activity would be more constrained. In contrast, our approach uses unfiltered future climate projections, allowing the full combination of temperature, humidity, and precipitation changes to influence ERC and fire behavior. We believe this to be a plausible, but not necessarily probable, pathway in which increased moisture offsets warming-driven fire risk in this humid pyrome.

Whether GCMs that more accurately simulate contemporary climate will also more reliably predict future climate remains an untestable hypothesis (Rupp et al. 2013). Nevertheless, by incorporating multiple GCMs and providing simulated burn probability through FSim and estimated burn probability based on empirical relationships, we not only address this uncertainty but also provide a basis for identifying potential areas of model consensus.

Influence of burn-day dynamics on fire activities

Both average fire size and the number of large fires contributed to changes in the total burned area, similar to findings from Dye et al. (2023). The former is mainly determined by the number of burn days (i.e., days when ERC exceeds the 80th percentile) and the latter is influenced by burn-day dynamics, including the number of burn days, the length of burn blocks, and the hours of burn in each day. In FSim, ERC percentiles determine the ignition of a fire (a fire can only ignite when daily ERC exceeds the 80th percentile) and daily burn hours (daily burn hours are 1, 3, and 5 h for ERC in the ranges of 80th–89th, 90th–96th, and 97th–100th percentiles, respectively, corresponding to burn days, high burn days, and extreme burn days). Because fire ignition probability is related to ERC via logistic regression in FSim (Andrews et al. 2003), the number of burn days (i.e., days when ERC exceeds the 80th percentile) is strongly related to the number of fires that ignite in FSim. Once a fire ignites, FSim has a built-in suppression algorithm designed to stop fire growth after encountering more than 2 consecutive non-burn days if the ignition occurred in a non-timber fuel type, or more than 7 consecutive burn days if ignition occurred in a timber fuel type. Therefore, the burn-day dynamics, along with the ignition location, fuel type, topography, winds, and landscape characteristics, work together to determine the growth and final size of a fire.

In contrast to the Western U.S., where ignited fires often spread rapidly and grow large under persistently dry and highly flammable conditions (Westerling et al. 2006), fires in the more humid Southeastern US require extended periods of consecutive days with elevated fire danger, as well as individual extreme burn days, to sustain active burning. The region's persistent high humidity and frequent, heavy rainfall events. This moisture rapidly wets the deep, heavy fuels, preventing the catastrophic, deep-burning fires commonly seen in the West (Blackmarr 1971). Our analysis reflects this distinction: additional burn-day metrics beyond the simple count of burn days help explain fire activities in this pyrome. In particular, the strong correlations between the number of large fires and both the number of burn days and extreme burn days indicate that, within FSim, fires must not only ignite but also experience sufficiently prolonged periods of high fire danger to exceed the large-fire threshold. Additionally, the significant relationship between the average length of burn blocks and total area burned highlights the importance of consecutive sequences of burn days in facilitating fire growth. Similar relationships between the number of burn days and burn probability have been documented in Southern California (Dye et al. 2023) and the Pacific Northwest (personal communication with

Dye et al. 2024), but the reliance on extended periods of consecutive days with elevated fire danger appears especially critical in this humid region.

Interpreting dry days as a localized indicator of fire potential

ERC, which determines burn days in FSim, approximates fuel dryness by integrating complex interactions among temperature, precipitation amount and duration, relative humidity, and solar radiation. We further dismantled the complexity of ERC and found that burn probability in this pyrome is more strongly associated with the combination of low relative humidity and limited precipitation. This finding is consistent with the sensitivity analysis over the conterminous US by Yu et al. 2023), which identified daily minimum relative humidity and precipitation as the most influential factors for predicting annual mean fire danger. While warmer temperatures generally promote drier conditions and are expected to increase in this region, temperature alone is not a reliable indicator of fire risk in the Southeast. For example, the highest temperatures typically coincide with the humid summer season, during which substantial precipitation suppresses fire activities. As a result, summer is not the typical peak fire season in this region (National Wildfire Coordinating Group, 2023).

To simplify risk assessment, our study introduces the concept of a "dry day" as a more practical alternative to the more intricate ERC (Cohen and Deeming 1985). This localized metric provides an effective means of evaluating fire risk in the region, particularly when accounting for known biases in climate models. For instance, evaluations of CMIP5-generation GCMs indicate that models such as bcc-csm1-1 exhibit a high precipitation bias over eastern North America (Sheffield et al. 2013; Maloney et al. 2014), which could lead to an underestimation of dry days and, in turn, fire risk, if relative humidity holds the same. While we do not propose replacing established fire danger indices such as KBDI or ERC, incorporating localized indicators like dry days can improve the accuracy and contextual relevance of fire risk assessments in this pyrome, especially under climate change scenarios where model uncertainties must be carefully interpreted.

While we found a significant correlation between the number of dry days and region-level burn probability, the influence of daily variations in meteorological variables, including temperature, relative humidity, and precipitation, and their interactions at finer temporal scales should not be overlooked. These dynamics play a critical role in shaping the temporal distribution of burn days and the length of continuous burn periods, or burn blocks. For example, the future projection from MIROC-ESM-CHEM shows a substantial increase in dry days compared to its historical period, yet the corresponding burn probability increases only slightly. Two factors may explain this discrepancy. First, many of the additional dry days may not lead to burn days due to unfavorable combinations of temperature, relative humidity, and precipitation. Second, even when dry days do result in burn days, they may be dispersed rather than consecutive, limiting their ability to sustain continuous burning.

Caveats and limitations of FSim

One limitation of FSim is its treatment of wind. The model draws wind vectors randomly from monthly joint distributions of wind speed and direction, producing conditions that are statistically representative but uncoupled from ERC or other daily meteorological variables. In addition, FSim applies a single wind vector for the full 24-h simulation period, preventing representation of sub-daily fluctuations that may meaningfully influence fire behavior.

Another important assumption in FSim is that the present-day relationship between ERC and ignition probability will remain constant in the future. In practice, ignition–ERC relationships vary across climate regimes and vegetation types and require local parameterization. As climate and vegetation conditions evolve, these relationships may shift in ways not captured by the current modeling framework (Riley and Loehman 2016).

A further caveat of our FSim simulations is that the spatial distribution and composition of vegetation types were held unchanged across both historical and future climate scenarios. This modeling choice was made to isolate the effects of climate change on fire behavior while minimizing the confounding influence of vegetation change. However, in reality, vegetation dynamics are expected to shift substantially over time due to interacting disturbances such as fire, drought, land use change, fire management practices, and the spread of invasive species. For instance, while increased precipitation may suppress wildfire risk in this humid region, it can also, along with elevated CO_2, accelerate tree growth and lead to greater fuel accumulation (Hanberry et al. 2024). With decreasing opportunities for prescribed burning, this accumulated biomass can elevate fire risk during subsequent drought events. The Southeastern US contains many fire-adapted ecosystems, such as longleaf pine savannas, which rely on frequent, low-intensity fires for maintenance. However, climate-driven disturbances and evolving fire management challenges may shift the distribution of dominant vegetation types—potentially reducing fire-adapted communities or facilitating the expansion of invasive species that alter fire behavior (Lippincott et al. 2000; Dillon et al. 2021). Moreover, different fire frequency scenarios—whether shaped by fire exclusion, prescribed burning, or wildfires—can result in varying levels of aboveground biomass, species composition, and fuel structure (Flanagan et al. 2019). As such, future research that integrates vegetation change models, land management strategies, and fire simulations will be critical for capturing the full spectrum of fire–climate–vegetation feedbacks in the Southeastern US.

Conclusions

Our study assessed the potential impacts of mid-twenty-first century climate change on wildfire activity in the Florida flatwoods pyrome using FSim, a spatially explicit fire behavior model driven by 9 GCM-based projections under the RCP8.5 scenario. By isolating the influence of climate from other interacting factors, we were able to examine how projected changes in fire weather affect burn probability, fire size, and the number of large fires. While it is not possible to create forecasts of future fire activity, only projections based on plausible future climate conditions, our simulations reveal key patterns and plausible shifts in fire regimes under a warming climate. Most GCMs projected an increase in burn probability and area burned, though the magnitude and spatial distribution of change varied across GCMs, underscoring the importance of embracing uncertainty when interpreting future fire risk. Importantly, we demonstrate that a negative change in either the number of fires or fire size is possible under a warming climate. Future convergence of GCM characteristics may resolve that uncertainty.

Our findings highlight the critical fire metrics, including burn days, extreme burn days, and the length of burn blocks, as drivers of fire activity in this fuel-rich, humid region. We also found that low relative humidity and limited precipitation, rather than temperature alone, are the strongest meteorological predictors of fire-conducive conditions. To enhance regional fire risk assessment, we introduced a "dry day" index as a simplified and practical alternative to more complex fire danger metrics like ERC.

Ultimately, our study demonstrates that future fire activity in this pyrome is likely to be variable and regionally nuanced. Rather than following a single narrative of increasing or decreasing fire risk, fire outcomes will depend on the interaction between climate variability, fire weather thresholds, and local vegetation and fuel conditions. Future modeling work that incorporates dynamic vegetation change and fire management practices will further improve our ability to characterize these complexities and support the development of resilient fire management and climate adaptation strategies tailored to the Southeastern U.S.

Abbreviations

ERC	Energy Release Component
FSim	Large Fire Simulator
GCM	Global Climate Models
IDG	Ignition Density Grid
KBDI	Keetch-Byram Drought Index
RAWS	Remote Automatic Weather Station
RCP	Representative Concentration Pathway
SOW	State Of Weather

Supplementary Information

The online version contains supplementary material available at https://doi.org/10.1186/s42408-026-00474-8.

Supplementary Material 1.

Acknowledgements

PG appreciates the discussion about the fire regime of this region with John A. Kupfer and J. Kevin Hiers. We also appreciate the comments from the anonymous reviewers.

Authors' contributions

PG, AWD, KLR, and JBK designed the study. PG conducted modeling and data analysis with the help of AWD. PG wrote the original draft. AWD, KLR, and JBK contributed to reviewing and editing.

Funding

This work was partially supported by the Research Momentum Fund, University of North Carolina Wilmington. This research was also supported in part by the Rocky Mountain Research Station and Pacific Northwest Research Station, Forest Service, U.S. Department of Agriculture (USDA). A. Dye was supported by a Joint Venture Agreement (22-JV-11261954-080) between the USDA Forest Service Western Wildland Environmental Threat Assessment Center and Oregon State University. The findings and conclusions in this paper are those of the author(s) and should not be construed to represent any official USDA or U.S. Government determination or policy.

Data availability

The data and material used in this research are partly available in the body of the article and appendices; other data/material is publicly available to all users upon a written request to the authors; all other data used are publicly available from their source.

Declarations

Ethics approval and consent to participate

Not applicable.

Consent for publication

Not applicable.

Competing interests

The authors declare no competing interests.

Author details

[1]Department of Earth and Ocean Sciences, University of North Carolina Wilmington, Wilmington, NC 28403, USA. [2]Department of the Oregon State Fire Marshal, Analytics & Intelligence Unit, Salem, OR 97302, USA. [3]Department of Forest Ecosystems & Society, Oregon State University, Corvallis, OR 97331, USA. [4]Missoula Fire Sciences Lab, USDA Forest Service Rocky Mountain Research Station, Missoula, MT 59808, USA. [5]USDA Forest Service Western Wildland Environmental Threat Assessment Center, Corvallis, OR 97331, USA.

Received: 5 September 2025 Accepted: 7 March 2026
Published online: 15 April 2026

References

Abatzoglou, J. T. 2013. Development of gridded surface meteorological data for ecological applications and modelling. *International Journal of Climatology* 33:121–131. https://doi.org/10.1002/joc.3413.

Abatzoglou, J. T., and T. J. Brown. 2012. A comparison of statistical downscaling methods suited for wildfire applications. *International Journal of Climatology* 32:772–780. https://doi.org/10.1002/joc.2312.

Abatzoglou, J. T., and C. A. Kolden. 2013. Relationships between climate and macroscale area burned in the western United States. *International Journal of Wildland Fire* 22:1003–1020. https://doi.org/10.1071/WF13019.

Ager, A. A., R. M. Houtman, M. A. Day, C. Ringo, and P. Palaiologou. 2019. Tradeoffs between US national forest harvest targets and fuel management to reduce wildfire transmission to the wildland urban interface. *Forest Ecology and Management* 434:99–109. https://doi.org/10.1016/j.foreco.2018.12.003.

Ager, A. A., A. M. G. Barros, R. Houtman, R. Seli, and M. A. Day. 2020. Modelling the effect of accelerated forest management on long-term wildfire activity. *Ecological Modelling* 421:108962. https://doi.org/10.1016/j.ecolmodel.2020.108962.

Ahlgrimm, M., and R. Forbes. 2014. Improving the representation of low clouds and drizzle in the ECMWF model based on ARM observations from the Azores. *Monthly Weather Review* 142:668–685. https://doi.org/10.1175/MWR-D-13-00153.1.

Andrews, P. L., D. O. Loftsgaarden, and L. S. Bradshaw. 2003. Evaluation of fire danger rating indexes using logistic regression and percentile analysis. *International Journal of Wildland Fire* 12 (2): 213–226. https://doi.org/10.1071/WF02059.

Archibald, S., C. E. R. Lehmann, J. L. Gómez-Dans, and R. A. Bradstock. 2013. Defining pyromes and global syndromes of fire regimes. *Proceedings of the National Academy of Sciences* 110 (16): 6442–6447. https://doi.org/10.1073/pnas.1211466110.

Balch, J. K., B. A. Bradley, J. T. Abatzoglou, R. C. Nagy, E. J. Fusco, and A. L. Mahood. 2017. Human-started wildfires expand the fire niche across the United States. *Proceedings of the National Academy of Sciences* 114 (11): 2946–2951. https://doi.org/10.1073/pnas.1617394114.

Barbero, R., J. T. Abatzoglou, N. K. Larkin, C. A. Kolden, and B. Stocks. 2015. Climate change presents increased potential for very large fires in the contiguous United States. *International Journal of Wildland Fire* 24:892–899.

Barnett, J. P. 1999. Longleaf pine ecosystem restoration: the role of fire. *Journal of Sustainable Forestry* 9 (1–2): 89–96. https://doi.org/10.1300/J091v09n01_07.

Barros, A. M., M. A. Day, H. K. Preisler, J. T. Abatzoglou, M. A. Krawchuk, R. Houtman, and A. A. Ager. 2021. Contrasting the role of human- and lightning-caused wildfires on future fire regimes on a Central Oregon landscape. *Environmental Research Letters* 16 (6) : 064081. https://doi.org/10.1088/1748-9326/ac03da.

Bayham, J., J. K. Yoder, P. A. Champ, and D. E. Calkin. 2022. The economics of wildfire in the United States. *Annual Review of Resource Economics* 14 (1): 379–401. https://doi.org/10.1146/annurev-resource-111920-014804.

Bedel, A. P., T. L. Mote, and S. L. Goodrick. 2013. Climate change and associated fire potential for the south-eastern United States in the 21st century. *International Journal of Wildland Fire* 22:1034–1043. https://doi.org/10.1071/WF13018.

Blackmarr, W. H. 1971. *Equilibrium moisture content of common fine fuels found in southeastern forests*. USDA Forest Service, Southeastern Forest Experiment Station. Research Paper SE-74.

Bowman, D. M. J. S., and F. H. Johnston. 2005. Fire smoke, fire management, and human health. *EcoHealth* 2 (1): 76–80. https://doi.org/10.1007/s10393-004-0149-8.

Bradshaw, L. S., and E. McCormick. 2009. *FireFamily Plus user's guide, version 4.0*. Boise, ID: USDA Forest Service, Fire and Aviation Management.

Brey, S. J., E. A. Barnes, J. R. Pierce, C. Wiedinmyer, and E. V. Fischer. 2018. Environmental conditions, ignition type, and air quality impacts of wildfires in the Southeastern and Western United States. *Earth's Future* 6 (8): 1442–1456. https://doi.org/10.1029/2018EF000972.

Brown, E. K., J. Wang, and Y. Feng. 2021. US wildfire potential: a historical view and future projection using high-resolution climate data. *Environmental Research Letters* 16 (3) : 034060. https://doi.org/10.1088/1748-9326/aba868.

National Interagency Coordination Center. 2024. *Wildland fire summary and statistics annual report 2024*. National Interagency Fire Center. https://www.nifc.gov/sites/default/files/NICC/2-Predictive%20Services/Intelligence/Annual%20Reports/2024/annual_report_2024.pdf.

Cohen, J. D., and J. E. Deeming. 1985. *The national fire-danger rating system: basic equations (Vol. 82)*. US Department of Agriculture, Forest Service, Pacific Southwest Forest and Range Experiment Station.

Dillon, W. W., D. Hiatt, and S. L. Flory. 2021. Experimental manipulation of fuel structure to evaluate the potential ecological effects of fire. *Forest Ecology and Management* 482:118884. https://doi.org/10.1016/j.foreco.2020.118884.

Dillon, G. K., J. H. Scott, M. R. Jaffe, J. Gilbertson-Day, M. P. Thompson, A. L. Freeborn, M. A. Finney, and S. S. Stevens-Rumann. 2023. *Spatial datasets of probabilistic wildfire risk components for the United States (270 m)*. 3rd Edition. Fort Collins, CO: Forest Service Research Data Archive. https://doi.org/10.2737/RDS-2016-0034-3.

Donovan, V. M., R. Crandall, J. Fill, and C. L. Wonkka. 2023. Increasing large wildfire in the eastern United States. *Geophysical Research Letters* 50 (24) : e2023GL107051. https://doi.org/10.1029/2023GL107051.

Duffield, J. W., C. J. Neher, D. A. Patterson, and A. M. Deskins. 2013. Effects of wildfire on national park visitation and the regional economy: a natural experiment in the Northern Rockies. *International Journal of Wildland Fire* 22:1155–1166. https://doi.org/10.1071/WF12170.

Dye, A. W., J. B. Kim, A. McEvoy, F. Fang, and K. L. Riley. 2021. Evaluating rural Pacific Northwest towns for wildfire evacuation vulnerability. *Natural Hazards* 107 (1): 911–935. https://doi.org/10.1007/s11069-021-04615-x.

Dye, A. W., P. Gao, K. Riley, J. B. Kim, T. Lei, and L. Yocom. 2023. High-resolution wildfire simulations reveal complexity of climate change impacts on projected burn probability for Southern California. *Fire Ecology* 19 (1): 1–19. https://doi.org/10.1186/s42408-023-00179-2.

Dye, A. W., M. J. Reilly, A. McEvoy, R. Lemons, K. L. Riley, J. B. Kim, and B. K. Kerns. 2024. Simulated future shifts in wildfire regimes in moist forests of Pacific Northwest, USA. *Journal of Geophysical Research-Biogeosciences* 129 (2) : e2023JG007722. https://doi.org/10.1029/2023JG007722.

Fill, J. M., C. N. Davis, and R. M. Crandall. 2019. Climate change lengthens southeastern USA lightning-ignited fire seasons. *Global Change Biology* 25:3562–3569. https://doi.org/10.1111/gcb.14727.

Finney, M. A., I. C. Grenfell, and C. W. McHugh. 2009. Modeling containment of large wildfires using generalized linear mixed-model analysis. *Forest Science* 55 (3): 249–255. https://doi.org/10.1093/forestscience/55.3.249.

Finney, M. A., C. W. McHugh, I. C. Grenfell, K. L. Riley, and K. C. Short. 2011. A simulation of probabilistic wildfire risk components for the continental United States. *Stochastic Environmental Research and Risk Assessment* 25 (7): 973–1000. https://doi.org/10.1007/s00477-011-0462-z.

Finney, M. A., I. C. Grenfell, B. Deryl, and E. Noonan-Wright. 2025. A generalized wildfire containment algorithm. *Ecological Modelling* 505:111134. https://doi.org/10.1007/s00477-011-0462-z.

Flanagan, S. A., S. Bhotika, C. Hawley, G. Starr, S. Wiesner, J. K. Hiers, J. J. O'Brien, S. Goodrick, M. A. Callaham, R. M. Scheller, K. D. Klepzig, and E. L. Loudermilk. 2019. Quantifying carbon and species dynamics under different fire regimes in a southeastern US pineland. *Ecosphere* 10 (6) : e02772. https://doi.org/10.1002/ecs2.2772.

Gaither, C. J., N. C. Poudyal, S. Goodrick, J. M. Bowker, S. L. Malone, and J. Gan. 2011. Wildland fire risk and social vulnerability in the Southeastern United States. *Forest Policy and Economics* 13:24–36. https://doi.org/10.1016/j.forpol.2010.07.009.

Gao, P., A. J. Terando, J. A. Kupfer, J. M. Varner, M. C. Stambaugh, T. L. Lei, and J. K. Hiers. 2021. Robust projections of future fire probability for the conterminous United States. *Science of the Total Environment* 789 : 147872. https://doi.org/10.1016/j.scitotenv.2021.147872.

Guyette, R. P., M. C. Stambaugh, D. C. Dey, and R.-M. Muzika. 2012. Predicting fire frequency with chemistry and climate. *Ecosystems* 15:322–335. https://doi.org/10.1007/s10021-011-9512-0.

Hamilton, M., C. Evers, M. Nielsen-Pincus, and A. Ager. 2024. Matching the scales of planning and environmental risk: an evaluation of Community Wildfire Protection Plans in the western US. *Regional Environmental Change* 24 (2) : 93. https://doi.org/10.1007/s10113-024-02239-y.

Hanberry, B., M. D. Abrams, and G. J. Nowacki. 2024. Potential interactions between climate change and land use for forest issues in the Eastern United States. *Land* 13 (3) : 398. https://doi.org/10.3390/land13030398.

Heidari, H., M. Arabi, and T. Warziniack. 2021. Effects of climate change on natural-caused fire activity in Western U.S. national forests. *Atmosphere* 12 (8) : 981. https://doi.org/10.3390/atmos12080981.

Hoffman, J. S., S. G. McNulty, C. Brown, K. D. Dello, P. N. Knox, A. Lascurain, C. Mickalonis, G. T. Mitchum, L. Rivers III, M. Schaefer, G. P. Smith, J. S. Camp, and K. M. Wood. 2023. Ch. 22. Southeast. In *Fifth national climate assessment*. Crimmins, A.R., C.W. Avery, D.R. Easterling, K.E. Kunkel, B.C. Stewart, and T.K. Maycock, Eds. U.S. Global Change Research Program, Washington, DC, USA. https://doi.org/10.7930/NCA5.2023.CH22

Huard, D., J. Fyke, I. Capellán-Pérez, H. D. Matthews, and A. I. Partanen. 2022. Estimating the likelihood of GHG concentration scenarios from probabilistic integrated assessment model simulations. *Earth's Future* 10 (10) : e2022EF002715. https://doi.org/10.1029/2022EF002715.

Knorr, W., F. Dentener, J. F. Lamarque, L. Jiang, and A. Arneth. 2017. Wildfire air pollution hazard during the 21st century. *Atmospheric Chemistry and Physics* 17 (14): 9223–9236. https://doi.org/10.5194/acp-17-9223-2017.

Kreider, M. R., P. E. Higuera, S. A. Parks, W. L. Rice, N. White, and A. J. Larson. 2024. Fire suppression makes wildfires more severe and accentuates impacts of climate change and fuel accumulation. *Nature Communications* 15 (1) : 2412. https://doi.org/10.1038/s41467-024-46702-0.

Kruskal W. H. and Wallis W. A. 1952. Use of ranks in one-criterion variance analysis. *Journal of the American Statistical Association* 47: 583–621. https://doi.org/10.1080/01621459.1952.10483441.

Kupfer, J. A., A. J. Terando, P. Gao, C. Teske, and J. K. Hiers. 2020. Climate change projected to reduce prescribed burning opportunities in the south-eastern United States. *International Journal of Wildland Fire* 29 (9): 764–778. https://doi.org/10.1071/WF19198.

Kupfer, J. A., K. Lackstrom, J. M. Grego, K. Dow, A. J. Terando, and J. K. Hiers. 2022. Prescribed fire in longleaf pine ecosystems: fire managers' perspectives on priorities, constraints, and future prospects. *Fire Ecology* 18 (1) : 27. https://doi.org/10.1186/s42408-022-00151-6.

LANDFIRE. 2018. *Homepage of the LANDFIRE Project*. U.S. Department of Agriculture, Forest Service and U.S. Department of the Interior, U.S. Geologic Survey. http://www.landfire.gov/index.php.

Levene, H. 1960. Robust tests for equality of variances. In *Contributions to probability and statistics: essays in honor of Harold Hotelling*, ed. I. Olkin, S. G. Ghurye, W. Hoeffding, W. G. Madow, and H. B. Mann, 278–292. Stanford (CA): Stanford University Press.

Lippincott, C. L. 2000. Effects of Imperata cylindrica (L.) Beauv.(cogongrass) invasion on fire regime in Florida sandhill (USA). *Natural Areas Journal* 20 (2): 140–149.

Liu, Y., S. L. Goodrick, and J. A. Stanturf. 2013. Future US wildfire potential trends projected using a dynamically downscaled climate change scenario. *Forest Ecology and Management* 294:120–135. https://doi.org/10.1016/j.foreco.2012.06.049.

Maloney, E. D., S. J. Camargo, E. Chang, B. Colle, R. Fu, K. L. Geil, Q. Hu, X. Jiang, N. Johnson, K. B. Karnauskas, and J. Kinter. 2014. North American climate in CMIP5 experiments: part III: assessment of twenty-first-century projections. *Journal of Climate* 27 (6): 2230–2270. https://doi.org/10.1175/JCLI-D-13-00273.1.

Marjani, M., and M. S. Mesgari. 2023. The large-scale wildfire spread prediction using a multi-kernel convolutional neural network. *ISPRS Annals of the Photogrammetry, Remote Sensing and Spatial Information Sciences* 10:483–488. https://doi.org/10.5194/isprs-annals-X-4-W1-2022-483-2023.

McEvoy, A., B. K. Kerns, and J. B. Kim. 2021. Hazards of risk: identifying plausible community wildfire disasters in low-frequency fire regimes. *Forests* 12 (7) : 934. https://doi.org/10.3390/f12070934.

Mitchell, R. J., Y. Liu, J. J. O'Brien, K. J. Elliott, G. Starr, C. F. Miniat, and J. K. Hiers. 2014. Future climate and fire interactions in the southeastern region of the United States. *Forest Ecology and Management* 327:316–326. https://doi.org/10.1016/j.foreco.2013.12.003.

Mote, P. W., L. Brekke, P. Duffy, and E. Maurer. 2011. Guidelines for constructing climate scenarios. *EOS Transactions, American Geophysical Union* 92 (31) : 258. https://doi.org/10.1029/2011eo310001.

National Wildfire Coordinating Group (NWCG). 2023. *Fire season climatology*. PMS 437. Available at: https://www.nwcg.gov/publications/pms437/weather/fire-season-climatology. Accessed 7 Dec 2025.

Nepal, S., L. Y. Pomara, N. P. Gould, and D. C. Lee. 2023. Wildfire risk assessment for strategic forest management in the southern United States: a Bayesian network modeling approach. *Land* 12 (12) : 2172. https://doi.org/10.3390/land12122172.

Parisien, M.-A., D. A. Dawe, C. Miller, C. A. Stockdale, and O. B. Armitage. 2019. Applications of simulation-based burn probability modelling: a review. *International Journal of Wildland Fire* 28 (12): 913–926. https://doi.org/10.1071/WF19069.

Paveglio, T., M. S. Carroll, and P. J. Jakes. 2008. Alternatives to evacuation—protecting public safety during wildland fire. *Journal of Forestry* 106 (2): 65–70.

Peterson, G. C. L., S. E. Prince, and A. G. Rappold. 2021. Trends in fire danger and population exposure along the wildland–urban interface. *Environmental Science & Technology* 55 (23): 16257–16265.

Platt, W. J. 1999. Southeastern pine savannas. *The savanna, barren, and rock outcrop communities of North America*, 23–51.

Pomara, L. Y., Gould, N. P., Nepal, S., Emmett, K. D., Goodrick, S. L., Lee, D. C. 2025. *Fire: an analysis to support the southern forest outlook*. Gen. Tech. Rep. SRS-280. Asheville, NC: U.S. Department of Agriculture, Forest Service, Southern Research Station. 57. https://doi.org/10.2737/SRS-GTR-280.

Prestemon, J. P., U. Shankar, A. Xiu, K. Talgo, D. Yang, E. Dixon, D. McKenzie, and K. L. Abt. 2016. Projecting wildfire area burned in the south-eastern United States, 2011–60. *International Journal of Wildland Fire* 25 (7): 715–729. https://doi.org/10.1071/WF15124.

Radeloff, V. C., D. P. Helmers, H. A. Kramer, M. H. Mockrin, P. M. Alexandre, A. Bar-Massada, V. Butsic, T. J. Hawbaker, S. Martinuzzi, A. D. Syphard, and S. I. Stewart. 2018. Rapid growth of the US wildland–urban interface increases wildfire risk to homes. *Proceedings of the National Academy of Sciences* 115 (13): 3314–3319.

Riley, K. L., and R. A. Loehman. 2016. Mid-21st century climate changes increase predicted fire occurrence and fire season length, Northern Rocky Mountains, United States. *Ecosphere* 7 (11) : e01543. https://doi.org/10.1002/ecs2.1543.

Riley, K. L., J. T. Abatzoglou, I. C. Grenfell, A. E. Klene, and F. A. Heinsch. 2013. The relationship of large fire occurrence with drought and fire danger indices in the western USA, 1984–2008: the role of temporal scale. *International Journal of Wildland Fire* 22:894–909. https://doi.org/10.1071/WF12149.

Riley, K. L., M. P. Thompson, J. H. Scott, and J. W. Gilbertson-Day. 2018. A model-based framework to evaluate alternative wildfire suppression strategies. *Resources* 7 (1) : 4. https://doi.org/10.3390/resources7010004.

Riley, K. L., S. N. Zimmer, E. Kodra, I. C. Grenfell, G. K. Dillon, J. H. Scott, M. R. Jaffe, J. H. Olszewski, K. C. Vogler, M. A. Finney, K. C. Short, W. M. Jolly, and S. E. Brittain. 2025. *Spatial datasets of probabilistic wildfire risk components for the conterminous United States (270m) for circa 2011 climate and projected future climate circa 2047*. Updated 01 July 2025. Fort Collins, CO: Forest Service Research Data Archive. https://doi.org/10.2737/RDS-2025-0006.

Robbins, Z. J., E. L. Loudermilk, T. G. Mozelewski, K. Jones, and R. M. Scheller. 2024. Fire regimes of the Southern Appalachians may radically shift under climate change. *Fire Ecology* 20 (1) : 2. https://doi.org/10.1186/s42408-023-00231-1.

Rother, M. T., J. M. Huffman, C. H. Guiterman, K. M. Robertson, and N. Jones. 2020. A history of recurrent, low-severity fire without fire exclusion in southeastern pine savannas, USA. *Forest Ecology and Management* 475:118406. https://doi.org/10.1016/j.foreco.2020.118406.

Rupp, D. E., J. T. Abatzoglou, K. C. Hegewisch, and P. W. Mote. 2013. Evaluation of CMIP5 20th century climate simulations for the Pacific Northwest USA. *Journal of Geophysical Research: Atmospheres* 118 (19): 10884–10906. https://doi.org/10.1002/jgrd.50843.

Scott, J. H., and R. E. Burgan. 2005. Standard fire behavior fuel models: a comprehensive set for use with Rothermel's surface fire spread model. *General technical report RMRS-GTR-153*. Fort Collins, CO: USDA Forest Service, Rocky Mountain Research Station. https://doi.org/10.2737/RMRS-GTR-153.

Scott, J. H., M. A. Finney, D. E. Calkin, and K. L. Gilbertson-Day. 2016. Examining alternative fuel management strategies and the relative contribution of National Forest System land to wildfire risk to adjacent homes – a pilot assessment on the Sierra National Forest, California, USA. *Forest Ecology and Management* 362:29–39. https://doi.org/10.1016/j.foreco.2015.11.038.

Scott, J. H., K. C. Short, M. Finney, J. Gilbertson-Day, and K. C. Vogler. 2018. *FSim: the large-fire simulator — guide to best practices version 0.3.1*. https://pyrologix.com/wp-content/uploads/2019/11/FSimBestPractices_0.3.1.pdf.

Shankar, U., J. P. Prestemon, D. McKenzie, K. Talgo, A. Xiu, M. Omary, B. H. Baek, D. Yang, and W. Vizuete. 2018. Projecting wildfire emissions over the south-eastern United States to mid-century. *International Journal of Wildland Fire* 27 (5): 313–328. https://doi.org/10.1071/WF17116.

Sheffield, J., A. P. Barrett, B. Colle, D. Nelun Fernando, R. Fu, K. L. Geil, Q. Hu, J. Kinter, S. Kumar, B. Langenbrunner, and K. Lombardo. 2013. North

American climate in CMIP5 experiments. Part I: evaluation of historical simulations of continental and regional climatology. *Journal of Climate* 26 (23): 9209–9245. https://doi.org/10.1175/JCLI-D-12-00592.1.
Short, K. C. 2014. A spatial database of wildfires in the United States, 1992–2011. *Earth System Science Data* 6 (1): 1–27. https://doi.org/10.5194/essd-6-1-2014.
Short, K. C. 2021. *Spatial wildfire occurrence data for the United States, 1992–2018 [FPA_FOD_20210617]*. 5th Edition. Fort Collins, CO: Forest Service Research Data Archive. https://doi.org/10.2737/RDS-2013-0009.5.
Short, K. C., I. C. Grenfell, K. L. Riley, and K. C. Vogler. 2020. Pyromes of the conterminous United States. *Forest Service Research Data Archive, Fort Collins, CO.* https://doi.org/10.2737/RDS-2020-0020.
SILVIS Lab. (n.d.). *Wildland–urban interface (WUI) change*. Available at: https://silvis.forest.wisc.edu/data/wui-change/. Accessed 12 Dec 2025.
Stevens-Rumann, C., and P. Morgan. 2016. Repeated wildfires alter forest recovery of mixed-conifer ecosystems. *Ecological Applications* 26:1842–1853. https://doi.org/10.1890/15-1521.1.
Student. 1908. The probable error of a mean. *Biometrika* 6:1–25.
Sun, Y., S. Solomon, A. Dai, and R. W. Portmann. 2006. How often does it rain? *Journal of Climate* 19:916–934. https://doi.org/10.1175/JCLI3672.1.
Sun, J., W. Qi, Y. Huang, C. Xu, and W. Yang. 2023. Facing the wildfire spread risk challenge: where are we now and where are we going? *Fire* 6 (6) : 228. https://doi.org/10.3390/fire6060228.
Terando, A., J. K. Hiers, M. Williams, S. L. Goodrick, and J. J. O'Brien. 2021. Is there a dry season in the Southeast US? *Global Change Biology* 27:713–715. https://doi.org/10.1111/gcb.15399.
Thompson, M. P., K. L. Riley, D. Loeffler, and J. R. Haas. 2017. Modeling fuel treatment leverage: encounter rates, risk reduction, and suppression cost impacts. *Forests* 8 (12): 469. https://doi.org/10.3390/f8120469.
Wang, S.S.-C., Y. Qian, L. R. Leung, and Y. Zhang. 2021. Identifying key drivers of wildfires in the contiguous US using machine learning and game theory interpretation. *Earth's Future* 9 (6) : e2020EF001910. https://doi.org/10.1029/2020EF001910.
Westerling, A. L., H. G. Hidalgo, D. R. Cayan, and T. W. Swetnam. 2006. Warming and earlier spring increase western U.S. forest wildfire activity. *Science* 313 (5789): 940–943. https://doi.org/10.1126/science.1128834.
Yu G., Feng Y., Wang J., and Wright D. B. 2023. Performance of fire danger indices and their utility in predicting future wildfire danger over the conterminous United States. *Earth's Future* 11(11): e2023EF003823. https://doi.org/10.1029/2023EF003823.
Zakari, R. Y., O. A. Malik, and O. Wee-Hong. 2025. An enhanced wildfire spread prediction using multimodal satellite imagery and deep learning models. *Remote Sensing Applications: Society and Environment* 29:101632. https://doi.org/10.1016/j.rsase.2025.101632.
Zhang, D., W. Wang, Y. Xi, J. Bi, Y. Hang, Q. Zhu, Q. Pu, H. Chang, and Y. Liu. 2023. Wildfire worsens population exposure to PM2.5 pollution in the continental United States. *Research Square*: rs-3. https://doi.org/10.21203/rs.3.rs-3345091/v2.

Publisher's Note